Biosystems Engineering 270 (2026) 104555

Contents lists available at ScienceDirect

Biosystems Engineering

journal homepage: www.elsevier.com/locate/issn/15375110

Research Paper

Analytical solutions for sprinkler irrigation uniformity under idealised uniform radial water application rate: comparison of square and equilateral triangular layouts

Giorgio Baiamonte *, Girolamo Vaccaro

Department of Agricultural, Food and Forest Sciences (SAAF), University of Palermo, viale delle Scienze, Bldg. 4, Palermo, 90128, Italy

A R T I C L E I N F O

Keywords:
Analytical solutions
Christiansen's uniformity coefficient
Uniform water application rate
Sprinkler radial patterns
Efficiency analysis

A B S T R A C T

Solid-set sprinkler irrigation systems are widely used in arid and semi-arid regions due to their ability to achieve uniform water application and support automation. However, accurate design is essential to optimise water use and energy efficiency. This study presents a novel analytical approach for assessing sprinkler performance under an idealised uniform radial pattern of water application rate (*RP-WAR*), considering both square and equilateral triangular layouts. Partial overlap areas were derived to determine weighted statistics, including Christiansen's uniformity coefficient (*CU*). For both sprinkler layouts, the dimensionless overlap fractions (*OF*) and sprinkler spacings required to achieve target *CU* values of 90 and 95 % were determined. A target *CU* of 95 % is achieved at *OF* values of 0.555 and 0.640 for square and equilateral triangular layouts, respectively, whereas a *CU* of 90 % corresponds to *OF* values of 0.546 and 0.441. Using 20 *CU* data from the literature, the procedure was verified, resulting in a relative error ranging from −7.70 % to 3.57 %. Under different *RP-WAR* scenarios and sprinkler layouts, efficiency indices were introduced to quantify the trade-offs between the required number of sprinklers and energy savings, with a normalisation procedure that facilitates comparative analysis. Weighted aggregation (single-index) and Pareto-ranking methods provided complementary approaches for sprinkler decision-making, alongside crop uniformity requirements and soil hydraulic properties. Results showed that uniform *RP-WAR* generally maximise energy efficiency, while convex patterns show higher efficiency than concave patterns in both square and equilateral triangular layouts.

Nomenclature

Symbols	
a	Halved normalised sprinkler interspace, s_*
a_i	General partial area associated with the triangle, as part of *RA*
A_H	Normalised hexagon reference area
A_i	General partial area associated with the reference area
A_S	Normalised square reference area
CU	Christiansen's uniformity coefficient
CU_{lit}	Christiansen's uniformity from literature
CU_H	Christiansen's coefficient for equilateral triangular layouts
CU_S	Christiansen's uniformity for square layouts
CV	Coefficient of variation
CV_H	Coefficient of variation for equilateral triangular layouts
CV_S	Coefficient of variation for square layouts
d	Euclidean distance
EI	Overall efficiency index
EI_{EN}	Efficiency index related to energy saving
EI_{EN*}	Normalised value of EI_{EN}
EI_{SP}	Efficiency index related to the required number of sprinklers
EI_{SP*}	Normalised value of EI_{SP}
h	Water application rate (mm h^{-1})
h_0	Water application rate at the sprinkler location (mm h^{-1})
h_H	Vector of overlapped *WAR* for equilateral triangular layouts
h_S	Vector of overlapped *WAR* for square layouts
h_{RA}	Mean water application rate associated with the reference area
h_{WR}	Mean water application rate of the isolated sprinkler
IS	Integration step
m	Parameter depending on a
M	Mean water application rate for $h_0 = 1$ mm h^{-1} (mm h^{-1})
M_H	Mean water application rate for equilateral triangular layouts
M_S	Mean water application rate for square layouts
n	Parameter depending on a
N	Number of sprinklers
N_m	Number of meshes along the radial direction

(*continued on next page*)

* Corresponding author.
E-mail addresses: giorgio.baiamonte@unipa.it (G. Baiamonte), girolamo.vaccaro@unipa.it (G. Vaccaro).

https://doi.org/10.1016/j.biosystemseng.2026.104555
Received 21 January 2026; Received in revised form 20 July 2026; Accepted 21 July 2026

(*continued*)

OF	Overlap fraction normalised with respect to the wetted radius
OF_{th}	Threshold normalised overlap fraction for full coverage
$OF_{th,x}$	Threshold normalised overlap fraction along x–x, for four partial areas (S)
$OF_{th,y}$	Threshold normalised overlap fraction along y–y, for three partial areas (H)
$OF_{th,7}$	Threshold normalised overlap fraction for $N < 7$ sprinklers
$OF_{th,9}$	Threshold normalised overlap fraction for $N < 9$ sprinklers
OV	Overlap of the wetted radius (m)
p	Maximum number of overlaps in the partial areas
RA	Reference area
RA_H	Hexagon reference area for equilateral triangular layouts
RA_S	Square reference area for square layouts
r	Radial distance from the sprinkler (m)
r_*	Radial distance from the sprinkler normalised by the wetted radius
S	Spacing between sprinklers (m)
S_*	Spacing between sprinklers normalised to the wetted radius
S_{*th}	Threshold normalised sprinkler spacing associated with OF_{th}
w_{EN}	Weight of the energy saving
WR	Wetted radius
w_{SP}	Weight of the required number of sprinklers
α	Parameter that describes different RP
$\Psi_{S,1}$	Arctangent function associated with square layouts
$\Psi_{S,2}$	Arctangent function associated with square layouts
$\Psi_{S,3}$	Arctangent function associated with square layouts
$\Psi_{S,4}$	Arctangent function associated with square layouts
$\Psi_{S,1}$	Arctangent function associated with equilateral triangular layouts
$\Psi_{S,2}$	Arctangent function associated with equilateral triangular layouts
$\Psi_{H,3}$	Arctangent function associated with equilateral triangular layouts
Abbreviations	
H	Hexagon
RP	Radial pattern
RP-WAR	Radial pattern of the water application rate
S	Square
WAR	Water application rate

1. Introduction

Solid-set sprinkler irrigation systems are particularly well-suited to arid and semi-arid regions, where irrigation requirements are high. Their relatively simple operation and strong potential for automation, combined with the ability to achieve uniform and efficient water application, can enhance farm profitability (Tarjuelo, Montero, Honrubia, et al., 1999). However, compared with other systems, such as microirrigation (Baiamonte et al., 2024), sprinkler irrigation is more prone to evaporative losses during application, particularly under windy and high-temperature conditions and when high operating pressures produce finer droplets (Carriço et al., 2025). In addition, its adoption requires careful consideration of pressurisation energy requirements and relatively high initial installation costs (Keller & Bliesner, 1990).

Water application uniformity is a key performance criterion in solid-set sprinkler irrigation systems, as it directly affects crop yield (Abd El-Wahed et al., 2016; Nascimento et al., 2019; Salmerón et al., 2012), water distribution, runoff, infiltration, and erosion (Chen, Li, Wang, & Song, 2023; Singh & Su, 2022). However, under specific conditions, a certain level of non-uniformity may be acceptable, for example, in dry sub-humid climates (Li & Rao, 2003) or for crops with a curvilinear water production function, such as cotton (Mateos et al., 1997).

Two of the most commonly used indicators for evaluating uniformity are Christiansen's uniformity coefficient (*CU*), which is based on the mean absolute deviation (Christiansen, 1942), and the distribution uniformity coefficient (*DU*), defined as the ratio of the average depth in the least watered 25 % of the area to the overall average depth (Merriam & Keller, 1978). Among these, *CU* remains the most widely adopted metric for assessing application uniformity and for identifying suitable sprinkler spacing, largely because it provides a practical benchmark for verifying whether a system complies with accepted performance standards (Christiansen, 1942; Keller & Bliesner, 1990).

In general, high application uniformity is achieved through appropriate overlap of individual sprinkler patterns, which depends on sprinkler spacing and layouts, wetted radius, *WR*, and radial pattern of the water application rate, *RP-WAR* (Fukui et al., 1980; Rezayati et al., 2023; Zhu et al., 2024). However, wind speed is the main uncontrollable environmental factor affecting sprinkler irrigation performance, as it can distort the spatial water distribution pattern and thereby reduce application uniformity (Dechmi et al., 2003; Keller & Bliesner, 1990; Seginer, 1987; Tarjuelo, Montero, Carrion, et al., 1999).

Both *RP-WAR* and *WR* are influenced by several sprinkler and operating characteristics, including sprinkler type, nozzle size, operating pressure, diffuser tooth length, riser height, and discharge angle (Hussain et al., 2024; Pan et al., 2024; Tarjuelo, Montero, Valiente, et al., 1999; Zhang et al., 2013).

Estimating sprinkler application uniformity requires characterising the spatial distribution of applied water depths, commonly through catch-can measurements at discrete sampling locations (Merriam & Keller, 1978). Although this approach has been widely used to evaluate the effects of operating pressure, sprinkler spacing and other design variables on uniformity metrics (Hussain et al., 2024; Li et al., 2022; Qureshi et al., 2023; Stambouli et al., 2014; Zhang et al., 2013), experimental characterisation over a broad range of conditions remains labour-intensive, time-consuming, and logistically demanding.

In recent decades, the *CU* has been increasingly estimated using modelling approaches that reduce or even avoid extensive catch-can field testing. In particular, several methods have been developed for this purpose, such as process-based and simulation models, data-driven approaches, and empirical and semi-empirical formulations (García Bandala et al., 2022; Playán et al., 2006, 2024; Robles et al., 2019; Skhiri et al., 2023).

In process-based and simulation models, Li et al. (2015) developed and validated a process-based modelling approach that reconstructs single- and multiple-sprinkler application patterns under variable meteorological forcing by coupling droplet ballistic trajectories with an in-flight evaporation formulation. Furthermore, the mean applied depth and *CU* are derived through pattern overlap and compared against laboratory and field observations.

Similarly, Yang et al. (2024) developed a droplet-based modelling approach for hilly terrain by integrating a digital elevation model, droplet dynamics, and volume conservation to map droplet landing points and derive local application rates, achieving good agreement between simulated and experimental values.

In contrast, for a given sprinkler operating under fixed conditions, once the *WR* and *RP-WAR* have been defined either from catch-can measurements or from simulation models, Baiamonte and Vaccaro (2026) introduced a normalised numerical approach to evaluate water application uniformity in solid-set systems. Their method computes *CU*, *CV* and mean applied depth, *M*, over a newly defined reference area, *RA*, represented by a square for square layouts and a hexagon for equilateral triangular layouts. The *RP-WAR* was expressed in dimensionless form using a parabolic function controlled by a shape parameter, allowing convex, linear and concave patterns to be analysed. For both layouts, the approach was used to determine the normalised overlap fraction of wetted circles (*OF*) and the corresponding sprinkler spacing (S_*) required to achieve target uniformity levels ($CU \approx 90$ % and 95 %).

Although sprinkler irrigation uniformity has been widely investigated through experimental and theoretical approaches, an analytical formulation for uniform *RP-WAR* based on the actual overlap areas between wetted circles has not yet been developed. In addition, the relative performance of convex, linear, concave and uniform *RPs-WAR* under square and equilateral triangular layouts have not been compared from a design-oriented perspective.

To bridge these knowledge gaps, this study has three main objectives: i) to develop, for uniform *RP-WAR*, an analytical procedure for calculating the partial overlap areas and the corresponding statistics (*M*, *CV* and *CU*), for square and equilateral triangular layouts; ii) to validate the suggested approach using data from literature; and iii) to compare uniform and non-uniform *RPs-WAR* performance and sprinkler layouts by introducing new efficiency indices. These indices are related to the number of sprinklers and energy demand and are normalised to enable consistent comparison across configurations. Specifically, single-index weighted aggregation and Pareto-ranking methods were applied to provide a robust multi-criteria evaluation of sprinkler performance and support design-oriented decision-making.

2. Theoretical background

2.1. Normalised parameters and results from numerical analysis (parabolic RPs-WAR)

Baiamonte and Vaccaro (2026) developed a simple numerical procedure to determine the Christiansen uniformity coefficient, *CU*, for solid-set sprinkler layouts with square and equilateral triangular layouts, considering both convex and concave radial patterns, *RP*, of the water application rate, *WAR*. The procedure also includes the linear *RP-WAR* (triangular pattern along the wetted diameter) that can be obtained by imposing the shape parameter α equal to zero into the parabolic radial pattern of the water application rate:

$$h = \alpha\, r_*^2 - (h_0 + \alpha)\, r_* + h_0 \tag{1}$$

where $r_* = r/WR$ is the dimensionless radial distance from the sprinkler, with r (m) the dimensional radial distance, and *WR* (m) the wetted radius, h (mm h^{-1}) is the water application rate at r_*, h_0 (mm h^{-1}) is the *WAR* value assigned at the sprinkler location ($r_* = 0$), and α is the shape parameter accounting for convex ($\alpha < 0$), linear ($\alpha = 0$) or concave ($\alpha > 0$) *RPs-WAR*.

The use of r_* allowed the *WAR* uniformity results to be extended to sprinklers with any wetted radius. In the same way, fixing h_0 at 1 mm h^{-1} permitted *WAR* uniformity to be generalised to any h_0, given that h_0 operates exclusively as a scale factor and has no effect on *WAR* uniformity.

For any *RPs-WAR*, the circular wetted areas provided by the sprinklers require the overlap of wetted radii between adjacent sprinklers, especially for *RP-WAR* that exhibit a non-uniform decaying pattern (Pan et al., 2023). This commonly adopted practice is fundamental in compensating for the lower water depths at the outer edges of each sprinkler's range, ultimately contributing to a more efficient and effective irrigation system design. This explains why the overlap, *OV* (m), which is linked to the sprinkler spacing, *S* (m), is a critical parameter in designing and installing sprinkler irrigation systems. According to *WR* (m), *OV* was expressed as:

$$OV = WR - \frac{S}{2} \tag{2}$$

The overlap was also normalised with respect to the *WR*, yielding the overlap fraction *OF*:

$$OF = \frac{OV}{WR} = 1 - \frac{S_*}{2} = 1 - a \tag{3}$$

where S_* is the sprinkler spacing normalised with respect to *WR*, and $a = S_*/2$. If *OF* is imposed, e.g. in accordance with the guideline provided by Baiamonte and Vaccaro (2026), the S_* parameter equals:

$$S_* = 2\,(1 - OF) \tag{4}$$

When appropriately spaced, sprinklers ensure that each area receives sufficient water, preventing both overwatering and underwatering. The spacing depends on various factors, including the type of sprinkler, the available water pressure, and the *RP-WAR*. By overlapping sprinkler patterns, high uniformity distributions can be achieved, minimising dry spots and ensuring optimal plant growth.

Sprinkler layouts also play a crucial role. Baiamonte and Vaccaro (2026) studied separately the two commonly adopted square and equilateral triangular layouts to investigate the uniformity of water application rate, as summarised in the following sections.

For square layouts and a unit *WR*, Fig. 1a illustrates 9 sprinklers and the associated wetted circles. For example, a scenario with $OF \equiv OV = 0.2$ (i.e., $S_* = 1.6$, Eq. (4)). The figure also indicates the corresponding parameter $a = S_*/2 = 0.8$, which is useful to consider for further developments.

For an assigned S_* (or *OF*, Eq. (4)), Baiamonte and Vaccaro (2026) defined a normalised square reference area, RA_S, centred on each sprinkler and with a side length equal to S_*. This conceptual area, represented in Fig. 1a by the bold solid square, provides a standardised spatial framework for analysis.

The selected RA_S is advantageous because an individual square reference area can be associated with each sprinkler, effectively partitioning the entire irrigated area into multiple contiguous squares, as illustrated by the dotted-line squares in Fig. 1a, and directly associating the number of required sprinklers to RA_S (higher RA_S, lower #sprinklers). In addition, unlike the approaches of Merriam and Keller (1978) and Keller and Bliesner (1990), in which *CU* evaluations were determined within square areas whose vertices are defined by sprinkler positions (Fig. 1a, black dashed lines), the numerical procedure provides a representative assessment of distribution uniformity across the whole field, including edge zone, as it accounts for all contributions from the sprinklers. Consequently, the number of square reference areas corresponds directly to the number of sprinklers in the system, ensuring comprehensive coverage of the irrigated area.

To evaluate the *WAR* distribution in the RA_S, a square mesh grid was considered in the numerical procedure, with an area sufficiently large to encompass the wet radii of all nine sprinklers previously considered. An odd number of rows/columns was selected to ensure symmetry with respect to the origin (Fig. 1a), thus locating the central sprinkler at *O* (0,0).

To achieve a high resolution of *WAR* distribution uniformity within the reference area, *RA*, a high number of meshes along the radial direction, denoted as N_m, equal to 1001, which corresponds to the integration step, *IS*, was used:

$$IS = \frac{WR}{N_m} \tag{5}$$

This high resolution provided a detailed representation of the *WAR* distributions, and the impact of *N* on the *WAR* uniformity in the *RA* was investigated (not reported here), with respect to this *N* value (Zhang et al., 2018).

According to the superposition principle, the contribution of the nine sprinklers to the water depth in the RA_S was assessed by summing the individual *WAR* values within the *RA*. Results from this approach are inherently tied to the *OF* and the assumed *RP-WAR*.

In this work, to address the analytical analysis, under the simplifying assumption $h = \text{const}$ (i.e. uniform *WAR*), the partial overlap of irrigated areas within the triangle depicted in Fig. 1b, for $OF = 0.42$, was considered. For the selected *OF*, owing to symmetry, only four partial overlap areas need to be investigated. Indeed, as *OF* increases, the analysis becomes progressively more complex due to the larger number of partial overlap areas, approaching infinity for full overlap ($OF \sim 1$).

For equilateral triangular layouts, the normalised-numerical approach followed the same procedure as that summarised for square layouts. The reference area in this case was hexagonal, RA_H (Fig. 2a).

For a unit *WR*, $OF = 0.2$ (i.e. $S_* = 1.6$, Eq. (4)), Fig. 2a illustrates the corresponding scenario with 7 sprinklers. Like square layouts, the dimensionless radial distance from the sprinkler, r_*, enables the generalisation of results to sprinklers with any *WR*. Fig. 2a also graphs the triangle reference area whose vertices are defined by sprinkler positions (Fig. 2a, black dashed lines) used in other approaches (Keller & Bliesner, 1990; Merriam & Keller, 1978), differing from the RA_H considered here.

Like square layouts, the selected RA_H also had the advantage of being associated with each sprinkler, effectively partitioning the entire irrigated area into multiple contiguous hexagons.

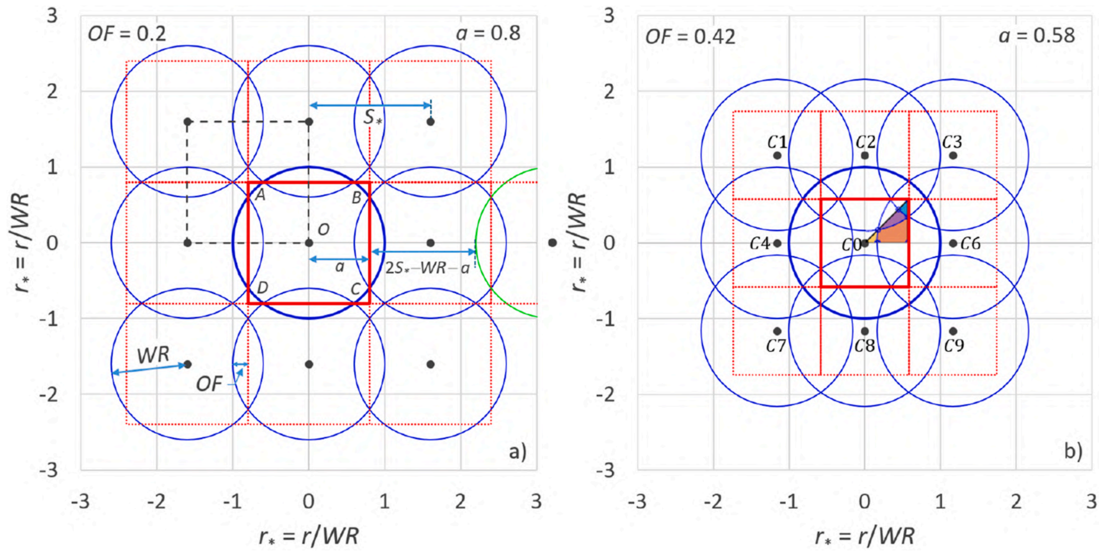

Fig. 1. Square layout for 9 sprinklers with $WR = 1$ m for a) $OF = 0.2$, and b) $OF = 0.42$, showing the four partially overlapped areas to be considered.

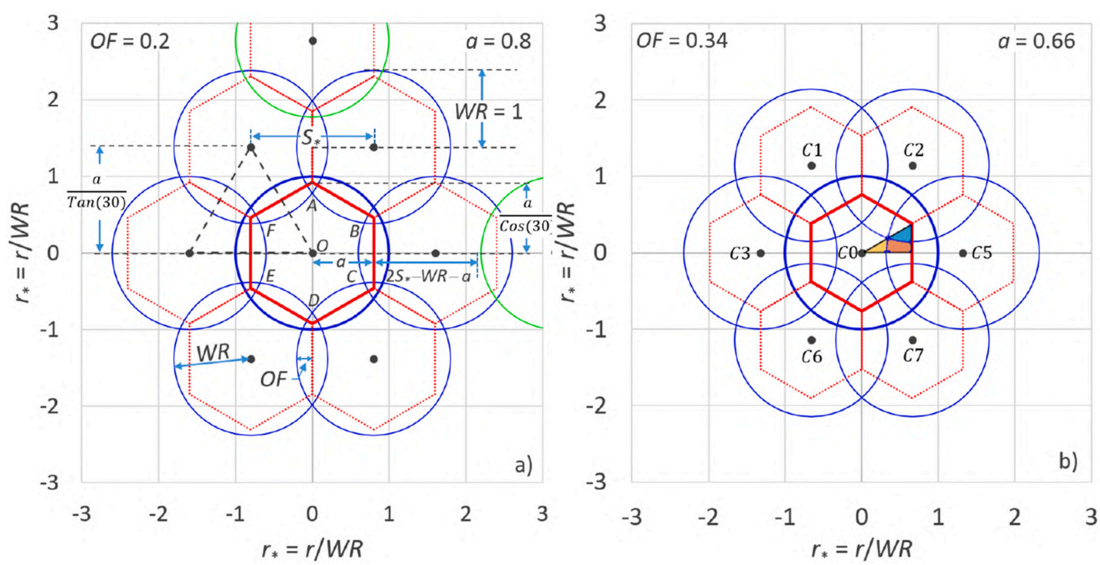

Fig. 2. Equilateral triangular layout for 7 sprinklers with $WR = 1$ m for a) $OF = 0.2$, and b) $OF = 0.34$, showing the three partial overlap areas to be considered.

Analogous to square layouts, Fig. 2b also displays the partial overlap of irrigated areas within the triangle, which will be considered for equilateral triangular layouts in further analysis. For the selected $OF = 0.34$, only three partial overlap areas occur, which simplifies the analytical derivation, although restricting the resulting solutions to the *OF* ranges detected in the following sections.

A drawback of the numerical procedure lies in the limited number of sprinklers considered in the analysis, $N = 9$ for square layouts and $N = 7$ for equilateral triangular layouts. This is because at increasing *OF*, *N* diverges; therefore, considering $N = 9$ and $N = 7$ sprinklers determine an underestimation of the water application rate. Although this condition is rarely assumed in practice, due to the very high number of sprinklers to be applied, with reference to the uniform *WAR* that in this work is considered, this assumption will be relaxed. Moreover, the *OF* thresholds, for which $N > 9$ and $N > 7$ sprinklers occur, respectively for square and equilateral triangular layouts, will be detected in the following sections.

The other limitations of the normalised-numerical procedure can be found as well in this work. Specifically, results are constrained by the structural parameters assumed when determining the *RP-WAR*. Factors such as nozzle diameter and rotational speed influence the *CV* and *CU* values calculated through the proposed methodology. However, since these influences are already embedded in the *RP-WAR* evaluation, the direct relationship between the structural parameters and the resulting *CV* and *CU* values remains unknown.

Additionally, the *CV* and *CU* results rely on the principle of superposition, which assumes that the water depth generated by multiple sprinklers operating simultaneously equals the sum of the depths produced by each one independently. Therefore, any potential interaction between jets from different sprinklers was disregarded.

Furthermore, the effects of wind, which are known to significantly alter the water application rate distribution (Dechmi et al., 2003; Keller & Bliesner, 1990), were not included in this analysis.

3. Materials and methods

This section presents the analytical procedure for determining the mean *WAR*, *M*, coefficient of variation, *CV*, and Christiansen uniformity coefficient, *CU*, under idealised uniform *RP-WAR* conditions, for both square and equilateral triangular layouts. The occurrence of an *OF* threshold, OF_{th}, which limits the applicability of the method, is identified; for *OF* values exceeding OF_{th}, a semi-analytical approach is proposed. For *RP-WAR* configurations that deviate from near-uniform conditions, the present methodology is not applicable, and only the numerical procedure developed by Baiamonte and Vaccaro (2026), which follows a similar framework to that adopted in this study, can be used.

3.1. OF thresholds for partial areas and a finite number of sprinklers

Different *OF* value characteristics that determine varying specific patterns of the partial overlap of irrigated areas are reported in Table 1.

The first one refers to the *OF* threshold, OF_{th}, at which the mean value for solid-set sprinklers equals that of the isolated sprinkler, which is discussed in Section 4.3.

The second set of OF_{th} corresponds to the condition in which the wetted circle circumscribes the individual influence area (square for square layouts and hexagon for equilateral triangular layouts), assuring full coverage of the reference areas, *RA*, and was already detected (Baiamonte & Vaccaro, 2026) and reported in Table 1 (second row).

The third OF_{th} refers to the condition for which more than four partial areas (for square layouts, Fig. 1b) and three partial areas (for equilateral triangular layouts, Fig. 2b) occur, denoted $OF_{th,x}$ and $OF_{th,y}$, respectively, within which the analytical solutions were derived.

The fourth and last OF_{th} refers to the contribution of more than nine sprinklers (for square layouts) and seven sprinklers (for equilateral triangular layouts), denoted $OF_{th,9}$ and $OF_{th,7}$. A part of the first *OF*s (first row, Table 1) will be discussed in Section 4.3; the other OF_{th} are detected in the next section separately, for square and equilateral triangular layouts.

3.1.1. Square layouts

For square layouts, the OF_{th} at which more than four partial areas occur (Fig. 1b), $OF_{th,x}$, is reached immediately by imposing $S_* = S_{*th,x} = WR = 1$ into Eq. (3), giving:

$$OF_{th,x} = 1 - \frac{S_{*th,x}}{2} = 0.5 \tag{6}$$

This is evident in Fig. 3a, which illustrates the wetted circles for $OF = 0.5$. For $OF > 0.5$ (i.e. $S_* < 1$), the contribution of the wetted circles centred in *C4* and in *C8* must also be considered, exceeding the four partial areas displayed in Fig. 1b, substantially complicating the analytical solutions due to the high number of partial areas.

For square layouts, because of the symmetry along the *x* and the *y* directions, OF_{th} value at which $N > 9$ sprinklers contribute to the RA_S, is equal, $OF_{th,x} = OF_{th,y}$. $OF_{th,x}$ can be derived by imposing the condition (see Fig. 1a):

$$\frac{S_{*,thx}}{2} = 2\,S_{*,thx} - WR - \frac{S_{*,thx}}{2} \tag{7}$$

where $S_{*,thx}$ is the normalised sprinkler interspace associated with $OF_{th,x}$. Considering Eq. (4), for unit *WR*, Eq. (7) provides:

$$OF_{th,9} = 1 - \frac{S_{*,thx}}{2} = 1 - \frac{WR}{3} = \frac{2}{3}WR = 0.667 \tag{8}$$

The wetted circles corresponding to this condition are displayed in Fig. 3b.

3.1.2. Equilateral triangular layouts

For equilateral triangular layouts, the OF_{th}, at which more than three partial areas (Fig. 2b) occur, needs to be searched along the *y* direction, namely $OF_{th,y}$, by imposing the condition:

$$\frac{S_{*th,y}}{2\tan 30} = WR \tag{9}$$

where $S_{*th,y}$ is the normalised interspace sprinkler associated with $OF_{th,y}$. Solving Eq. (9) and considering Eq. (3), for unit *WR*, Eq. (9) provides:

$$OF_{th,y} = 1 - \frac{1}{\sqrt{3}} \tag{10}$$

This case can be observed in Fig. 4a, where the wetted circles for $OF = 1 - 1/\sqrt{3}$ are illustrated. For $OF > 1 - 1/\sqrt{3}$ (i.e. $S_* < 2/\sqrt{3}$), the contribution of the wetted circle centred in *C7* must also be included, exceeding the three partial areas displayed in Fig. 2b.

The OF_{th} at which $N > 7$ sprinklers contribute to RA_H, namely $OF_{th,7}$, can be derived by imposing the condition:

$$\overline{AO} = \frac{S_{*th,7}}{Tan\,30^\circ} - WR \tag{11}$$

where $S_{*th,7}$ is the normalised interspace sprinkler associated with $OF_{th,7}$. Considering that $\overline{AO} = \frac{S_{*th,7}}{2\,Cos\,30^\circ}$, for unit *WR*, solving Eq. (11) provides $S_{*th,7}$ and the associated $OF_{th,7}$:

$$S_{*th,7} = \frac{\sqrt{3}}{2} \tag{12}$$

$$OF_{th,7} = 1 - \frac{\sqrt{3}}{4} = 0.566 \tag{13}$$

The wetted circles corresponding to $OF_{th,7}$ are displayed in Fig. 4b.

It is remarkable that results of *M*, *CV* and *CU* values obtained from numerical procedure for $OF > OF_{th,9}$, for square layouts, and for $OF > OF_{th,7}$, for equilateral triangular layouts, do not consider the sprinkler contributions to *RA* of $N > 9$ and $N > 7$ sprinklers; this drawback is relaxed in the following analysis that is differently addressed according the full *OF* range values reported in Table 1, following a so-called semi-analytical procedure.

In conclusion, to inspect sprinkler irrigation system performance under uniform *WAR*, three different procedure were applied (Table 2): i) the numerical solutions according the aforementioned *OF* thresholds, $OF_{th,9}$ and $OF_{th,7}$, ii) the semi-analytical solution based on the partial overlap areas in the entire *OF* range [0,1] and iii) the analytical solution according the *OF* thresholds, $OF_{th,x}$ and $OF_{th,y}$, in the *OF* ranges reported in Table 2.

Note that the semi-analytical solution is so denoted because it does not require mesh grids as employed in the numerical solutions and does not provide closed-form solutions. The latter is because the partial areas are assessed for any *OF* by using the polyarea function available for the MATLAB® code; thus, no error associated with the mesh grid size occurs, as in the numerical one.

Table 1
For square and equilateral triangular layouts, *OF* thresholds identifying the equality of solid-set and isolated sprinkler means, full coverage conditions, the formation of more than four and three overlap areas (preventing the analytical solutions), and the need to consider more than $N = 9$ and *7* sprinklers, respectively.

square layout				equilateral triangular layout				Note
OF	exact symbolic *OF*	S_*	*a*	*OF*	exact symbolic *OF*	S_*	*a*	
0.114	$1-\sqrt{\pi}/2$	1.772	0.886	0.048	$1/6\ [6-3^{3/4}\sqrt{(2\,\pi)}]$	1.905	0.952	OF_{th} thresholds at which the solid-set mean equals the isolated sprinkler mean
0.293	$1-1/\sqrt{2}$	1.414	0.707	0.134	$1-\sqrt{3}/2$	1.732	0.866	OF_{th} thresholds for full coverage (Baiamonte & Vaccaro, 2026)
0.5	1/2	1	0.5	0.422	$1-1/\sqrt{3}$	1.156	0.578	OF_{th} thresholds ($OF_{th,x}$ *and* $OF_{th,y}$) for *CV* and *CU* analytical solutions
0.667	2/3	0.666	0.333	0.567	$1-\sqrt{3}/4$	0.866	0.433	OF_{th} thresholds, $OF_{th,9}$ for $N = 9$ (square), and $OF_{th,7}$ for $N = 7$ (triangular) sprinklers

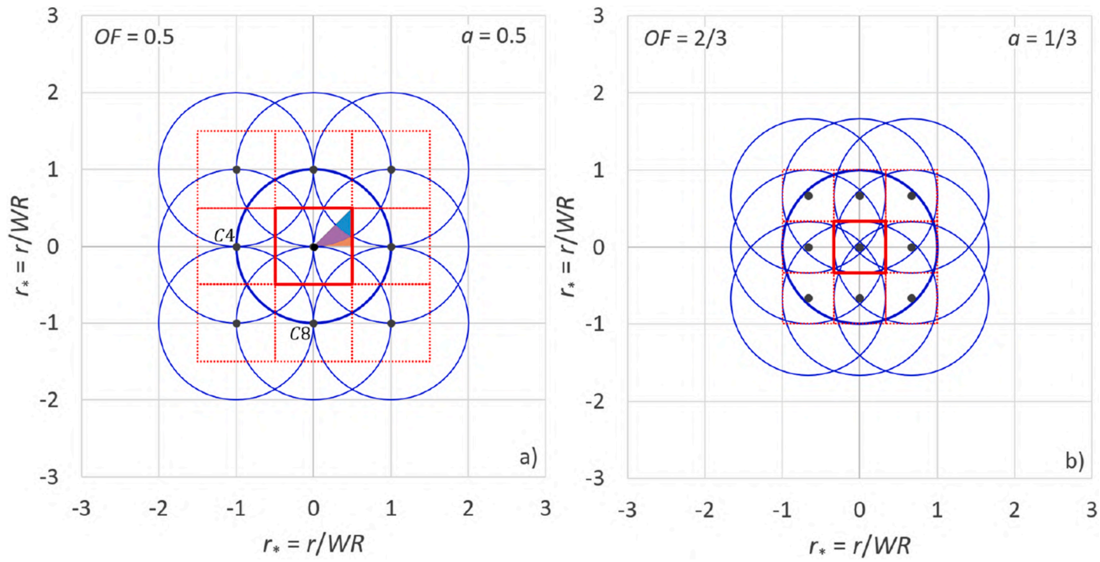

Fig. 3. Square layouts for 9 sprinklers with $WR = 1$ m for a) $OF = 05$, and b) $OF = 2/3$.

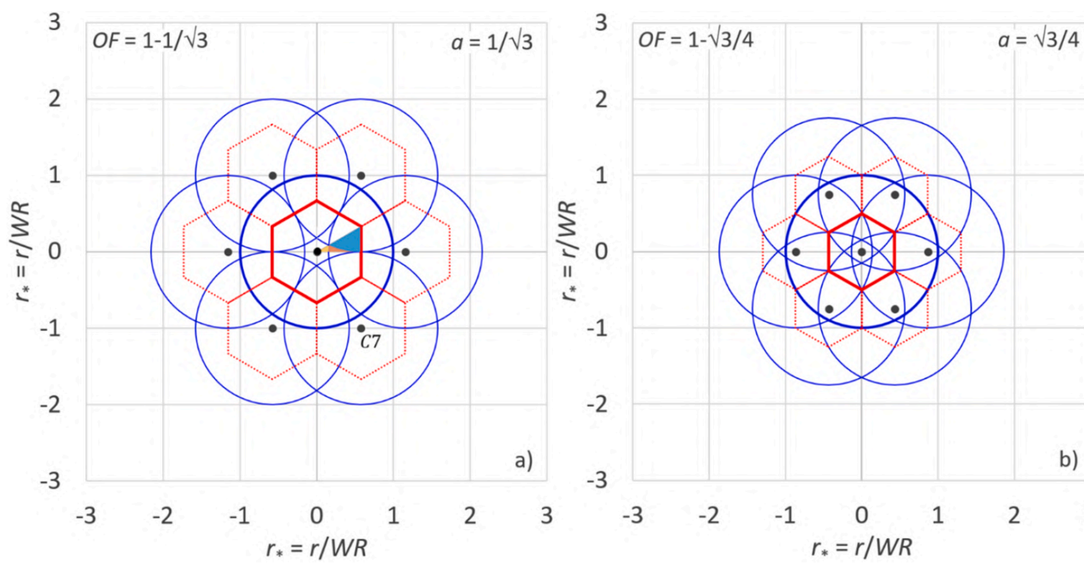

Fig. 4. Equilateral triangular layouts for 7 sprinklers with $WR = 1$ m for a) $OF = 1 - 1/\sqrt{3}$, and b) $OF = 1 - \sqrt{3}/4$.

Table 2
For square and equilateral triangular layouts, *OF* ranges for which the numerical, analytical and semi-analytical solutions have been applied. In brackets, exact symbolic value.

sprinklers' layouts	min *OF* limit		max *OF* limit		procedure
	value	exact symbolic *OF*	value	exact symbolic *OF*	
square layout	0	0	0.667	(2/3)	numerical
	0.293	$(1-1/\sqrt{2})$	0.5	(1/2)	analytical
	0	0	1	1	semi-analytical
equilateral triangular layout	0	0	0.567	$(1-\sqrt{3}/4)$	numerical
	0.134	$(1-\sqrt{3}/2)$	0.422	$(1-1/\sqrt{3})$	analytical
	0	0	1	1	semi-analytical

For deriving the analytical solutions, the partial overlap areas need to be formulated as illustrated in the following sections.

3.2. Determining the partial overlap areas for square layouts

3.2.1. Square layouts

Fig. 5 illustrates a zoomed portion of Fig. 1b, highlighting the four partial irrigated areas, a_1, a_2, a_3 and a_4, and the main dimensions required for the partial areas' derivation.

Of course, the analysis is developed for a_1, a_2, a_3 and a_4 and then, owing to the symmetry, the RA_S is obtained by multiplying the sum of these four partial areas by 8.

Before deriving the analytical solutions of the partial areas, some characteristics points need to be defined (Fig. 5). A part the axes origin *O* (0,0), *P*(*a*,*a*) and *P'* (*a*,0), which are already established, the coordinate of *I*, *I'*, *A*, *B*, and *Q* are derived in the following, first setting the

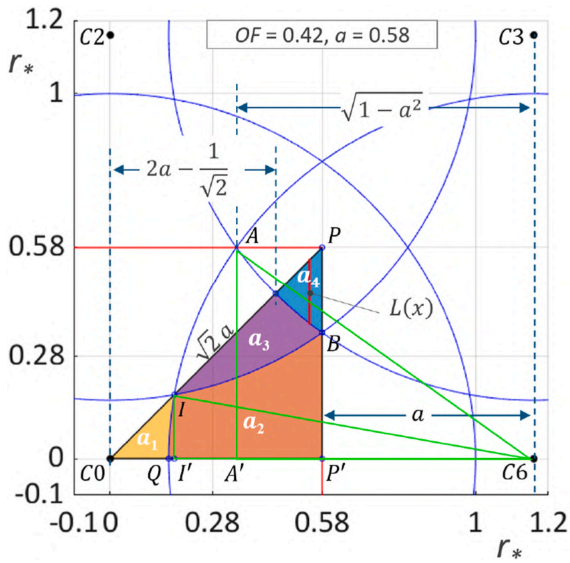

Fig. 5. For square layouts, partial irrigated areas, a_1, a_2, a_3 and a_4, for $OF = 0.42$ (see Fig. 1b).

parameters m and n that also recur in the partial-area solutions and in the corresponding statistics:

$$m = \sqrt{1-a^2}, n = \sqrt{1-2a^2} \tag{14}$$

To derive the coordinates of the point I, consider the wetted circle centred in $C6(2a,0)$:

$$(x-2a)^2 + y^2 = 1 \tag{15}$$

The interception point, I, lies on the bisector, $y = x$, which can be substituted in Eq. (15), giving:

$$(x-2\,a)^2 + x^2 = 1 \tag{16}$$

Solving Eq. (16) and considering the solution inside the triangle, with the minus sign, provides the coordinates of the point I, and therefore that of I', respectively:

$$I\left(a-\frac{n}{\sqrt{2}}, a-\frac{n}{\sqrt{2}}\right) \tag{17}$$

$$I'\left(a-\frac{n}{\sqrt{2}}, 0\right) \tag{18}$$

where n is defined by Eq. (14).

The ordinate of the point A, y_A, is equal to a that, substituted into Eq. (15) and considering the solution with the minus sign, with $a < 1$, gives $x_A = 2\,a - m$. Therefore, the A and the B symmetric coordinates can be written:

$$A(2a-m, a) \tag{19}$$

$$B(a, 2a-m) \tag{20}$$

where m is indicated in Eq. (14).

Finally, the coordinate of point Q (Fig. 1b) can be determined by imposing $y = 0$ into the equation describing the wetted circle centred in $C6(2a,0)$ (Eq. (15)), giving:

$$Q(2\,a-1, 0) \tag{21}$$

The abovementioned coordinates of the characteristic points, I, I', A, B, and Q, were needed to derive the analytical solutions of the partial areas. Derivations of the latter are reported in Appendix A, while in the following only the final solutions of the partial areas within the RA, A_1, A_2, A_3 and A_4, and of the appearing arctangent functions, are presented, respectively:

$$A_1 = 8\,a_1 = 4\left[\left(2\,a-\sqrt{2}\,n\right)a-\Psi_{S,1}\right] \tag{22}$$

$$A_2 = 8\,a_2 = 4\left[2\,\Psi_{S,1}-\left(m-2\sqrt{2}\,n\right)a-\Psi_{S,2}\right] \tag{23}$$

$$A_3 = 8\,a_3 = 4\left[\left(2\,(m-a)-\sqrt{2}\,n\right)a-\Psi_{S,1}+\Psi_{S,3}\right] \tag{24}$$

$$A_4 = 8\,a_4 = 4\left[\Psi_{S,4}-a\,(m-a)\right] \tag{25}$$

where the arctangent functions $\Psi_{S,1}, \Psi_{S,2}, \Psi_{S,3}$ and $\Psi_{S,4}$ are equal to:

$$\Psi_{S,1} = arctan\frac{\sqrt{2}\,a-n}{\sqrt{2}\,a+n} \tag{26}$$

$$\Psi_{s,2} = arctan\frac{a}{m} \tag{27}$$

$$\Psi_{S,3} = arctan\frac{2\,a\,(a+m)-1}{1-2\,a\,(a-m)} \tag{28}$$

$$\Psi_{S,4} = arctan\frac{m-a}{m+a} \tag{29}$$

For verification of the above-reported partial irrigated areas, it can be shown that the A_i summation exactly provides the RA of square layouts, RA_S:

$$RA_s = \sum_{i=1}^{4} A_i = S_*^2 = 4\,a^2 \tag{30}$$

In the next section, following the same framework, equilateral triangular layouts are addressed.

3.2.2. Equilateral triangular layouts

As in square layouts, Fig. 6 illustrates a zoomed portion of Fig. 2b, highlighting the three partial irrigated areas, a_1, a_2, and a_3, and the main dimensions required for the partial areas' derivations.

Again, the analysis is derived for the partial areas a_1, a_2, and a_3, and then, owing to the symmetry, RA_H is obtained by multiplying the sum of these three partial areas by 12.

First, the coordinates of some characteristic points need to be defined. Since the angle $P\hat{0}P'$ is 30°, $P(a, a/\sqrt{3})$, while the interception

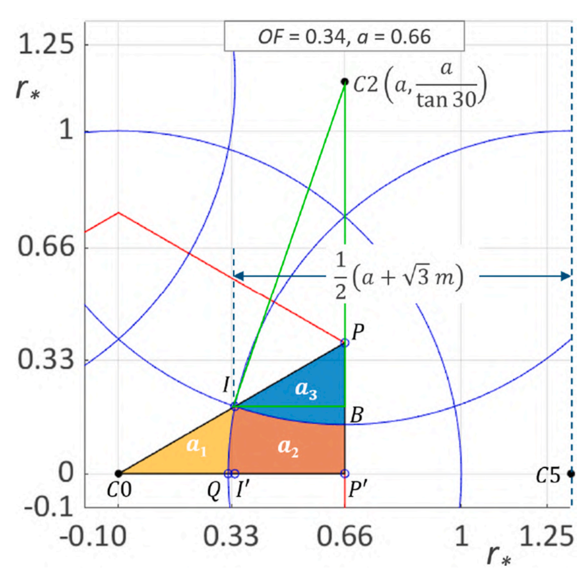

Fig. 6. For equilateral triangular layouts, partial irrigated areas, a_1, a_2, and a_3, for $OF = 0.34$ (see Fig. 2b).

point, I, lies in the line, $y = a/\sqrt{3}\,x$, which can be substituted in Eq. (15), providing the solution x_I, the corresponding y_I, derived by the same equation of the line, and the coordinate of the point I', respectively:

$$x_I = \frac{1}{2}\left(3a - \sqrt{3}\ m\right) \quad (31)$$

$$y_I = \frac{1}{2}\left(\sqrt{3}\ a - m\right) \quad (32)$$

$$I'\left(\frac{1}{2}\left(3a - \sqrt{3}\ m\right), 0\right) \quad (33)$$

The abovementioned coordinates of the characteristic points, I, I', A, B, and Q, were needed to derive the analytical solutions of the partial areas. Derivations of the latter are reported in Appendix B, while in the following only the final solutions of the partial areas within the RA_H, A_1, A_2, and A_3, and of the appearing arctangent functions, are presented, respectively:

$$A_1 = 12\,a_1 = 6\left[\left(\sqrt{3}\ a - m\right) a - \Psi_{H,1}\right] \quad (34)$$

$$A_2 = 12\,a_2 = 6\left[\Psi_{H,2} - \left(\sqrt{3}\ a - 2\,m\right) a\right] \quad (35)$$

$$A_3 = 12\,a_3 = 6\left[\Psi_{H,3} - \left(m - \frac{a}{\sqrt{3}}\right) a\right] \quad (36)$$

where the arctangent functions $\Psi_{H,1}$, $\Psi_{H,2}$ and $\Psi_{H,3}$ are equal to:

$$\Psi_{H,1} = \arctan\frac{\sqrt{3}\,a - m}{\sqrt{3}\,m + a} \quad (37)$$

$$\Psi_{H,2} = \arctan\frac{2\,a^2 - 1}{2\,a\,m} \quad (38)$$

$$\Psi_{H,3} = \arctan\frac{\sqrt{3}\,m - a}{\sqrt{3}\,a + m} \quad (39)$$

Again, for verification of the above-reported partial irrigated areas, it can be shown that the A_i summation provides the hexagonal RA of equilateral triangular layouts, RA_H:

$$RA_H = \sum_{i=1}^{3} A_i = \frac{\sqrt{3}}{2} S_*^2 = 2\sqrt{3}\,a^2 \quad (40)$$

3.2.3. Comparison of the partially irrigated areas

The derived partially irrigated overlap areas $A_S = \{A_1, A_2, A_3,$ and $A_4\}$, for square layouts, and $A_H = \{A_1, A_2,$ and $A_3\}$, for equilateral triangular layouts, make it possible to display the weighted partial areas vs. OF, with weight the corresponding overlap numbers, $h_S = \{1, 2, 3,$ and $4\}$, and $h_H = \{1, 2,$ and $3\}$, respectively, as illustrated in Fig. 7a and b. The considered OF ranges are those reported in Table 2, for which analytical solutions of CV and CU will be derived. Fig. 7a and b also plot the OF values corresponding to Fig. 5 and Fig. 6, respectively.

Interestingly, the partial areas with almost triangular shapes, associated with A_1, A_3, and A_4 for square layouts (Fig. 5) and A_1 and A_3 for equilateral triangular layouts (Fig. 6), exhibit a monotonic decreasing or increasing behaviour vs OF. In contrast, for the A_2 areas, associated with both sprinkler layouts and characterised by an almost quadrangular shape, a non-monotonic behaviour occurs, and an OF value corresponding to a maximum partial area could be detected (Fig. 7, brown lines).

Furthermore, in Fig. 7a and b, the weighted A_i summation provides in both cases the π value. The latter is not surprising, since it is a natural consequence of the framework introduced by Baiamonte and Vaccaro (2026), who defined a reference area, RA, associated with each sprinkler. Indeed, for unit WR, which allows the sprinkler geometry to be rescaled to any wetted radius, π represents the dimensionless circular wetted area, weighted with respect to the overlap numbers, h_S and h_H.

The ratio between π and RA must provide the mean WAR, M_S ($M_S = \pi/RA$). In other words, if the number of sprinklers equals that of the associated RA, the mean WAR only depends on the weighted partial areas.

A numerical example for square layouts may clarify this finding. Under uniform WAR, assume the sprinkler flow rate $q = 16\ \mathrm{L\ s^{-1}}$, and a radius of $WR = 30$ m. The WAR referred to the wetted circle of the isolated sprinkler, h_{WR}, results in:

$$h_{WR} = \frac{q}{\pi\ WR^2} = 20.37\ mm\ h^{-1} \quad (41)$$

The actual mean WAR that considers the contribution of the surrounding sprinklers must be referred to the RA and must be calculated by rescaling M_S, as:

$$h_{RA} = h_{WR}\ M_S = \frac{q}{\pi\ WR^2}\frac{\pi}{RA_S} = \frac{q}{WR^2 RA_S} = 44.44\ mm\ h^{-1} \quad (42)$$

where RA_S is the reference area associated with square layouts (Eq. (30)). As it is expected, the actual mean WAR, h_{RA}, is higher than h_{WR}, and of course depends on RA_S, thus on the sprinkler spacing, S. In Eq. (42), it was assumed $S = 0.6 \times 2\ WR$ (Amer, 2006), giving $S = 36$ m, $S_* = 1.2$, and the $RA_S = 1.44$ (Eq. (30)).

Of course, under unit WR, if $RA_s = S_*^2$ is imposed to be equal to the wetted circle area of the isolated sprinkler, $\pi\ WR^2$, S_* and OF_{th} result in:

$$S_* = \sqrt{\pi} \Rightarrow OF_{th} = 1 - \frac{\sqrt{\pi}}{2} \quad (43)$$

and the corresponding S is equal to 53.17 m, giving $h_{WR} = h_{RA}$ and $M_s = 1$, i.e. the solid-set sprinkler behaves as an isolated sprinkler, verifying the normalised procedure to assess h_{RA} from $M_S = \pi/RA_S$ (Eq.

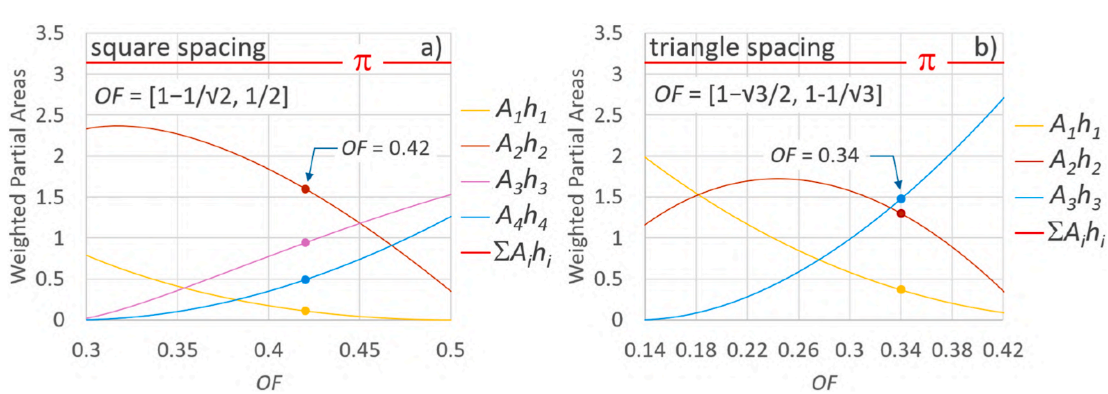

Fig. 7. Weighted partial irrigated areas vs. OF, a) for square layouts and b) for equilateral triangular layouts. The summation equal to π in both cases is also plotted. The OF values corresponding to Fig. 5 and Fig. 6 are also indicated.

(42)) (Table 1). This further OF_{th} limiting condition (Eq. (43)), together with that derivable for equilateral triangular layouts:

$$S_* = \frac{\sqrt{2}\,\pi}{3^{1/4}} \Rightarrow OF_{th} = \frac{1}{6}\left(6 - 3^{3/4}\sqrt{2\,\pi}\right) \tag{44}$$

is also reported in Table 1.

3.3. Statistics

The mean, M, the coefficient of variation, CV, and the Christiansen uniformity coefficient of WAR, CU, which are commonly considered the most widely used indicators to assess the solid-set sprinkler irrigation performance, were analysed. As previously assessed, the weighted mean must be considered, which for unit WR results in:

$$M = \frac{\sum_{i=1}^{p} A_i h_i}{\sum_{i=1}^{p} A_i} = \frac{\pi}{RA} \tag{45}$$

where the h_i (mm h^{-1}) is the WAR associated with the number of overlapped areas, and p is the index associated with the area irrigated the highest number of times:

$$h_i = \{h_1, h_2, \ldots, h_p\} = \{1, 2, \ldots, p\} \tag{46}$$

in the weighted standard deviation, σ, relationship, the average of squared differences of WAR with respect to the mean, M, must be weighted, with weight the partial area, A_i, and then divided by the sum of the weights:

$$\sigma = \sqrt{\frac{\sum_{i=1}^{p} A_i\,(h_i - M)^2}{\sum_{i=1}^{p} A_i}} \tag{47}$$

Eq. (47) makes it possible to denote the coefficient of variation, CV:

$$CV = \frac{\sigma}{M} = \frac{\sqrt{\frac{\sum_{i=1}^{p} A_i\,(h_i - M)^2}{\sum_{i=1}^{p} A_i}}\;\sum_{i=1}^{p} A_i}{\pi} = \frac{1}{\pi}\sqrt{\sum_{i=1}^{p} A_i\,(h_i - M)^2 \sum_{i=1}^{p} A_i} \tag{48}$$

in both RA_S and RA_H, the CU was calculated as (Christiansen, 1942):

$$CU = 100\,\frac{1 - \sum_{i=1}^{p}(A_i|h_i - M|)}{\sum_{i=1}^{p} A_i\,h_i} \tag{49}$$

Note that the statistics describing the WAR uniformity are not directly linked to the operating sprinkler characteristics (such as operating pressure head, nozzle shape and size, etc.). This is because the resulting statistics illustrated in the next section depend on the adopted RP-WAR, which itself is a consequence of those sprinkler characteristics.

In the following sections, based on the statistics defined above, the relationships of the partial areas are used to derive M, CV and CU analytical solutions, separately for square (Section 3.3.1.) and equilateral triangular (Section 3.3.2.) layouts.

3.3.1. Square layouts

For square layouts, using Eqs. (30) and (45), the mean WAR within the square reference area, M_S, is expressed as:

$$M_S = \frac{\pi}{RA_S} = \frac{\pi}{4\,a^2} \tag{50}$$

Based on the above considerations regarding the mean (Section 3.3), Eq. (50) can be used without any OF range limitations. In contrast, for the standard deviation, since the derived partial areas need to be applied, the OF range is that reported in Table 3 (analytical solution, $OF \in [1-1/\sqrt{2}, 0.5]$, with $1-1/\sqrt{2} = 0.293$).

Substituting the partial areas described by Eqs. (22), (23), (24), and (25) into Eq. (47), after simple but long algebra, the following solution was derived:

$$\sigma = \frac{1}{4\,a^2}\sqrt{\left(7\,\pi - 8\left(a\left(m + \sqrt{2}\,n\right) + \Psi_{S,1} + \Psi_{S,2}\right)\right)4\,a^2 - \pi^2} \tag{51}$$

from Eq. (51), the coefficient of variation for square layouts, CV_S, can be readily obtained (Eq. (48)):

$$CV_S = \frac{1}{\pi}\sqrt{\left(7\,\pi - 8\left(a\left(m + \sqrt{2}\,n\right) + \Psi_{S,1} + \Psi_{S,2}\right)\right)4\,a^2 - \pi^2} \tag{52}$$

To derive the Christiansen uniformity coefficient for square configurations, CU_S, three different cases can be distinguished. This is because the absolute value appearing in Eq. (49) does not allows to derive a unique relationship, as for CV_S (Eq. (52)), because the minus or plus sign depends on M_S, thus on a parameter ($S_*/2$) (Eq. (50)). In particular, the corresponding OF ranges can be derived by finding the OF values for which the difference ($h_s - M_s$) changes sign. Using Eqs. (3) and (50), setting this difference equal to zero, yields:

$$h_S - \frac{\pi}{4\,(1 - OF)^2} = 0 \tag{53}$$

Solving Eq. (53) with respect to OF provides:

$$OF = 1 \pm \frac{\sqrt{\pi}}{2\,\sqrt{h_S}} \tag{54}$$

Excluding the solution with the plus sign, giving $OF > 1$, with no physical meaning, for $h_S = \{1,\ 2,\ 3,\ \text{and}\ 4\}$, Eq. (54) provides $OF = \{0.114,\ 0.373,\ 0.488,\ \text{and}\ 0.557\}$. Considering the $OFs \in [0.293, 0.5]$ (Table 1), only $OF = 0.373$ and 0.488 (Fig. 8a) need to be considered; thus, the three OF ranges result in: [0.293, 0.373], [0.373, 0.488], and [0.488, 0.5]. The latter can be observed in Fig. 8a, where the difference ($h_S - M_S$) are plotted versus OF, for the four overlapped $WARs$.

Therefore, to derive CU_S solutions, when substituting the partial areas (Eqs. (22)–(25)) into Eq. (47), according to Fig. 8a, the ($h_S - M_S$) change of sign must be considered to maintain positive the difference ($h_S - M_S$), as imposed by the absolute value appearing in the Christiansen uniformity coefficient (Eq. (49)).

For $OF \in [0.293, 0.373]$, [0.373, 0.488], and [0.488, 0.5], Eqs. (55), (56), and (57) report the analytical solutions of the CU_S, obtained by substituting Eqs. (22), (23), (24), and (25) into Eq. (49), respectively:

$$CU_S = 100\left(1 - 2\left(\frac{1}{a^2} - \frac{4}{\pi}\right)\left(a\left(2\,a - \sqrt{2}\,n\right) - \Psi_{s,1}\right)\right) \tag{55}$$

Table 3
Overlap fraction, OF, normalised sprinkler spacing, S_*, parameter a, and reference area, RA, used to derive the statistics, M, CV, for $CU = 85$, 90 and 95 %. The table also reports the statistics corresponding to the threshold OF values (*), below which full coverage cannot be achieved.

sprinklers' layouts	OF	S_*	a	Ref Area, RA	M	CV	CU
square layouts	0.531	0.938	0.469	0.880	3.568	0.163	85.0
	0.546	0.909	0.454	0.826	3.803	0.130	90.0
	0.555	0.890	0.445	0.792	3.965	0.103	95.0
	0.293*	1.414	0.707	2.000	1.571	0.315	68.8
equilateral triangular layout	0.426	1.148	0.574	1.141	2.752	0.209	85.0
	0.441	1.118	0.559	1.082	2.904	0.187	90.0
	0.640	0.721	0.361	0.450	6.978	0.083	95.0
	0.134*	1.732	0.866	2.598	1.209	0.336	72.6

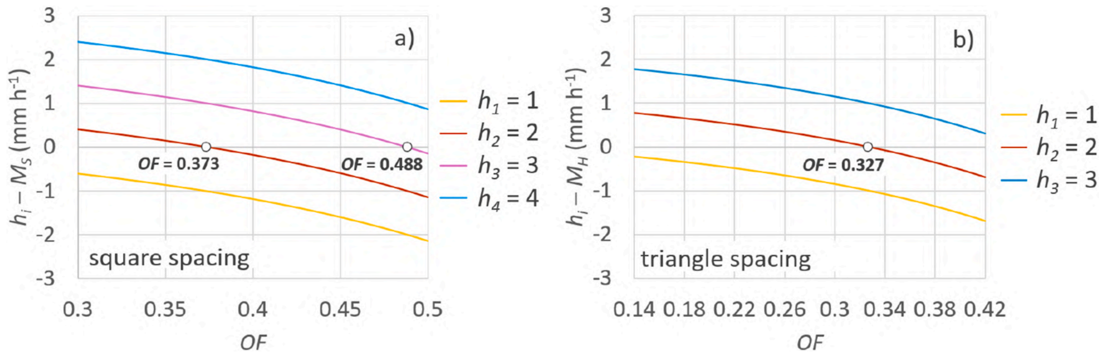

Fig. 8. Differences between a) the overlap number, $h_S = \{1, 2, 3, \text{and } 4\}$ and the weighted mean, for square layouts, M_S, and b) the overlap number, $h_H = \{1, 2, \text{and } 3\}$, and the weighted mean, for equilateral triangular layouts, M_H. Dots refer to the OF values where the differences change sign.

$$CU_S = 100\left[\begin{array}{c} 2\,\Psi_{S,1}\left(\dfrac{12}{\pi}-\dfrac{1}{a^2}\right)-2\,\Psi_{S,2}\left(\dfrac{8}{\pi}-\dfrac{1}{a^2}\right)+\dfrac{2}{a}\left(m-\sqrt{2}\,n\right) \\ +\dfrac{8\,a}{\pi}\left((a-m)2+3\sqrt{2}\,n\right)-3 \end{array}\right] \tag{56}$$

$$CU_S = 100\left(1-\left(\frac{1}{2\,a^2}-\frac{8}{\pi}\right)\left(4\,a\,(m-a)+4\,\Psi_{S,2}-\pi\right)\right) \tag{57}$$

where the arctangent functions $\Psi_{s,1}$ and $\Psi_{s,2}$ are defined by Eqs. (26) and (27).

For square layouts, Fig. 9 plot the mean, M_s (Fig. 9a), the coefficient of variation CV_S (Fig. 9b), and the Christian uniformity coefficient, CU_S (Fig. 9c), corresponding to i) the numerical solution, according to Baiamonte and Vaccaro (2026)'s procedure, ii) the semi-analytical procedure (i.e. statistics are derived by considering the partial areas from the MATLAB® polyarea function) and iii) the analytical procedure (Eqs. (50) and (52), and 55–59), in the above mentioned OF ranges, showing that generally they match from each other.

Discrepancies between the numerical and semi-analytical solutions appear for $OF > OF_{th,9}$ (white dots), because of the drawback of the numerical procedure that does not consider the contribution of $N > 9$ sprinklers in this OF range, as stated in Section 2.

3.3.2. Equilateral triangular layouts

For equilateral triangular layouts, using Eqs. (40) and (45), the mean of WAR within the hexagon reference area, M_H, is expressed as:

$$M_H = \frac{\pi}{RA_H} = \frac{\pi}{2\sqrt{3}\,a^2} \tag{58}$$

As for square layouts, Eq. (58) can be used without any OF range limitations. Conversely, for the standard deviation, since the derived partial areas need to be applied, the OF range is that reported in Table 3, $OF \in [1-\sqrt{3}/2,\ 1-1/\sqrt{3}]$, or in three digital places [0.134, 0.422].

Substituting the partial areas described by Eqs. (34), (35), and (36) into Eq. (47), the following solution was derived:

$$\sigma = \frac{1}{2\sqrt{3}\,a^2}\sqrt{12\sqrt{3}\,a^2\left(9\,\Psi_{H,3}+4\,\Psi_{H,2}-\Psi_{H,1}-2\,a\,m\right)-\pi^2} \tag{59}$$

Again, from Eq. (59), the coefficient of variation for equilateral triangular layouts, CV_H, can be readily obtained (Eq. (48)):

$$CV_H = \frac{1}{\pi}\sqrt{12\sqrt{3}\,a^2\left(9\,\Psi_{H,3}+4\,\Psi_{H,2}-\Psi_{H,1}-2\,a\,m\right)-\pi^2} \tag{60}$$

To derive the Christiansen uniformity coefficient for equilateral triangular layouts, CU_H, two different cases can be distinguished. Analogous to square layouts, the corresponding OF ranges can be derived by finding the OF values for which the difference $(h_H - M_H)$ changes sign (Fig. 8b). Using Eqs. (3) and (58), putting equal to zero such difference, yields:

$$h_H - \frac{\pi}{2\sqrt{3}\,(1-OF)^2} = 0 \tag{61}$$

Solving Eq. (61) with respect to OF provides:

$$OF = 1 \pm \frac{\sqrt{\pi}}{2\cdot 3^{1/4}} \tag{62}$$

Excluding again the solution with the plus sign, which yields $OF > 1$, for $h_H = \{1, 2, \text{and } 3\}$, Eq. (62) provides $OF = \{-0.347, 0.327, \text{and } 0.551\}$. Considering that $OF_H \in [0.134, 0.422]$ (Table 1), only $OF = 0.327$ needs to be taken into account; thus, the two OF ranges result in: [0.134, 0.327], and [0.327, 0.422]. The latter can be observed in Fig. 8b, where the difference $(h_H - M_H)$ are plotted versus OF, for the three $WARs$, h_H, associated with the three overlapped partial areas.

Therefore, to derive CU_H solutions, when substituting the partial areas (Eqs. (34)–(36)) into Eq. (49), according to Fig. 8b, the sign change

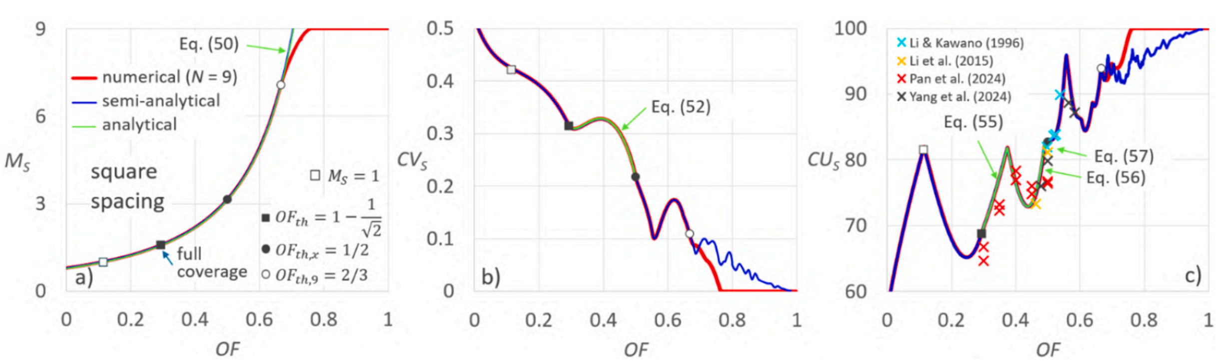

Fig. 9. For square layouts, a) mean WAR, M_S (mm h^{-1}), b) coefficient of variation, CV_S, and c) Christiansen uniformity coefficient, CU_S, versus OF. Numerical, semi-analytical, and analytical solutions are shown together with the OF thresholds (see Table 1).

of $(h_H - M_H)$ must be considered, to maintain positive the difference $(h_H - M_H)$ (Eq. (49)).

For $OF \in [0.134, 0.327]$ and $[0.327, 0.422]$, Eqs. (63) and (64) report the analytical solutions of the CU_H, obtained by substituting Eqs. (34), (35), and (36) into Eq. (49), respectively:

$$CU_H = 100 \left[1 - \frac{1}{\pi a^2}\begin{pmatrix} 12a^3\left(m - \sqrt{3}a\right) + a\pi\left(5a - 2\sqrt{3}m\right) + \left(6a^2 - \sqrt{3}\pi\right)\Psi_{H,1} + \\ -\left(\sqrt{3}\pi - 12a^2\right)\Psi_{H,2} - \left(\sqrt{3}\pi - 18a^2\right)\Psi_{H,3}\end{pmatrix}\right] \tag{63}$$

$$CU_H = 100 \left[1 - \frac{1}{\pi a^2}\begin{pmatrix} 12a^3\left(\sqrt{3}a - 3m\right) - a\pi\left(a - 2\sqrt{3}m\right) + \left(6a^2 - \sqrt{3}\pi\right)\Psi_{H,1} + \\ +\left(\sqrt{3}\pi - 12a^2\right)\Psi_{H,2} - \left(\sqrt{3}\pi - 18a^2\right)\Psi_{H,3}\end{pmatrix}\right] \tag{64}$$

where the arctangent functions $\Psi_{H,1}$, $\Psi_{H,2}$, and $\Psi_{H,3}$ are defined by Eqs. (37), (38), and (39).

For equilateral triangular layouts, Fig. 10 plots the mean, M_H (Fig. 10a), the coefficient of variation CV_H (Fig. 10b), and the Christian uniformity coefficient, CU_H (Fig. 10c), corresponding to i) the numerical solution according to Baiamonte and Vaccaro (2026)'s procedure, ii) the semi-analytical procedure, and iii) the analytical procedure (Eqs. (58), (60), (63) and (64)), in the above mentioned *OF* ranges, showing that generally they match from each other.

As for square layouts, for $OF > OF_{th,9}$ (white dots), discrepancies between the numerical and semi-analytical solutions occur because of the drawback of the numerical procedure that does not consider the contribution of $N > 7$ sprinklers in such *OF* range, as stated in Section 2.

From a practical point of view, design solutions are those corresponding to high *CV*s and high *CU*s. Under uniform *WAR*, for square and equilateral triangular layouts, Table 3 reports the *OF* and S_* values to be applied to achieve satisfying *CU* values, specifically $CU = 85$, 90 and 95 %. Table 3 also reports the statistics corresponding to the threshold *OF* values (*), below which full coverage cannot be achieved, which exactly match those derived numerically by Baiamonte and Vaccaro (2026, see Table 4 , last row).

Note that for equilateral triangular layouts, high CU_H may also occur at very low *OF* (Fig. 10c), which could appear convenient from an economic point of view because a smaller number of sprinklers would be required. However, this condition could not be recommended for two reasons: i) *OF* is less than the threshold assuring full coverage ($OF_{th} = 0.134$, square dot, Fig. 10c), and ii) the corresponding CV_H, which considers the no-irrigated area, and also provides a robust measure of *WAR* uniformity, is very high (Fig. 10b).

The sprinkler interspace, S_*, normalised with respect to wetted radius, *WR*, together with the corresponding means, *M*, enable the solid-set sprinkler design to be generalised for any desired *WR* and *WAR*. The application performed in the next section helps clarify how to move from dimensionless to dimensional design parameters in practice.

4. Results and discussion

The following section presents the results obtained by applying the proposed analytical and semi-analytical procedure. First, the procedure is validated against experimental data from the literature for square sprinkler layouts (Section 4.1). The validated approach is then used i) to determine the values of CU_S based on the design recommendations of Keller and Bliesner (1990), and ii) to compare the *OF* values required to achieve a target of $CU_S = 90$ % with the corresponding recommendations, for both square and equilateral triangular layouts under different *RPs-WAR* (Section 4.2). Finally, a comprehensive comparison of sprinkler system performance across layouts and *RP-WAR* is carried out using the proposed efficiency indices and multi-criteria ranking methods (Section 4.3).

4.1. Application and experimental validation

The radial pattern of the water application rate, *RP-WAR*, and the wetted radius, *WR*, are influenced by several sprinkler and operating characteristics, including sprinkler type, nozzle size, operating pressure, diffuser tooth length, riser height, and discharge angle (Hussain et al., 2024; Pan et al., 2024; Tarjuelo, Montero, Valiente, et al., 1999; Zhang et al., 2013). For a given sprinkler operating under fixed conditions, the *WR* and the *RP-WAR* can be determined either from catch-can measurements (Merriam & Keller, 1978) or by means of simulation models (Li et al., 2015). Once these quantities are known, the proposed analytical/semi-analytical procedure can be applied to uniform *RP-WAR*, while the numerical approach of Baiamonte and Vaccaro (2026) can be used for parabolic *RPs-WAR* to determine the *OF* required to achieve a target *CU*.

To assess the suitability of the proposed procedure for square layouts, experimental nearly uniform *RPs-WAR* reported in the literature were used as example applications. Specifically, nine experimental cases were selected from Li and Kawano (1996, three runs), Li et al. (2015, two runs), Pan et al. (2024, two runs), and Yang et al. (2024, two runs), including different operating pressures, which determined different *WR*, and, in the case of Pan et al. (2024), different diffuser tooth lengths. These studies are particularly appropriate for this purpose because they provide measured radial water application profiles and the corresponding *CU* values for different square layouts, allowing direct comparison with the results obtained using the proposed procedure.

The selected studies cover different aspects of sprinkler irrigation performance. Li and Kawano (1996) analysed sprinkler rotation non-uniformity in commercial sprinkler products and its effect on *CU* in overlapped water distribution patterns. Li et al. (2015) developed and validated droplet-dynamics and evaporation models to simulate droplet trajectories and water distribution from measured radial profiles at

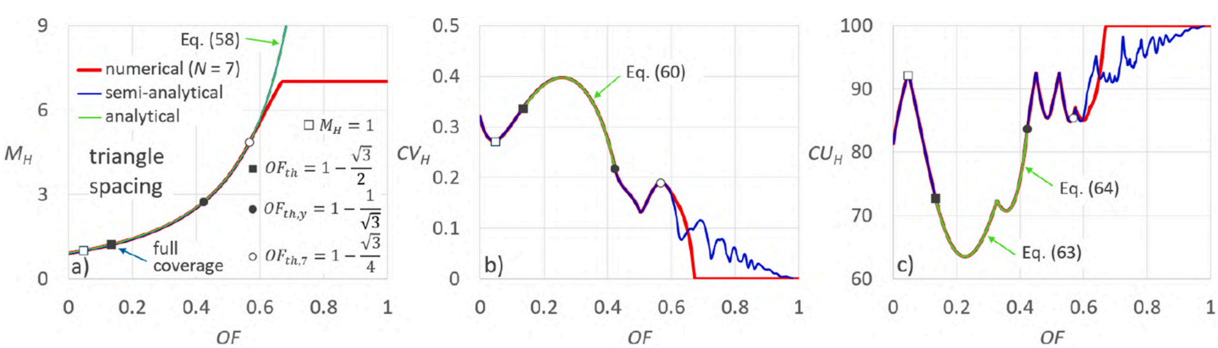

Fig. 10. For equilateral triangular layouts, a) mean *WAR*, M_H (mm h^{-1}), b) coefficient of variation, CV_H, and c) Christiansen uniformity coefficient, CU_H, versus *OF*. Numerical, semi-analytical and analytical solutions are shown together with the *OF* thresholds (see Table 1).

different operating pressures.

Pan et al. (2024) investigated the combined effect of operating pressure and diffuser tooth length on *RP-WAR*, identifying cases with a relatively uniform pattern. Yang et al. (2024) proposed a droplet-based modelling approach for flat and hilly terrain by integrating digital elevation data, droplet dynamics, and volume conservation to estimate droplet landing positions and local application rates.

The selected *RP-WAR* measurements were carried out under indoor conditions, excluding wind and evaporation processes, thus aligning with the assumptions made in this work and making these experimental results well-suited as example applications of the procedure proposed herein, as the authors also provided the values of the uniformity coefficient, *CU*.

Fig. 11a–d shows the nearly uniform *RPs-WAR* selected from the literature. Specifically, the profiles from Li and Kawano (1996, Fig. 11a), Li et al. (2015, Fig. 11b), and Yang et al. (2024, Fig. 11d) correspond to different pressure heads. For the selected profiles from Pan et al. (2024, Fig. 11c), the adopted pressure head was the same, while the diffuser tooth length was varied, as indicated by letters B and C in the legend.

Table 4 summarises operating pressure head, *P*, wetted radius, *WR*, and square sprinkler spacing, *S*, adopted in the selected experimental studies. The corresponding overlap fraction, *OF* (Eq. (3)), which the suggested procedure requires, together with the dimensionless spacing, S_* (Eq. (4)), are also reported. Cases for which the analytical procedure could not be applied because *OF* exceeded its limiting value, i.e., $OF = 0.5$ (Table 1), are indicated with an asterisk. In addition, Table 4 provides the *OF* range used to select the appropriate analytical solution (Eqs. (55) and (56) or 57) for calculating CU_S.

For the same *OF* values reported in Table 4, Table 5 provides the other derived geometric step-by-step parameters ($a = S_*/2$, m, n, $\Psi_{s,1}$, $\Psi_{s,2}$), together with the values of CU_S, *CU* from literature, CU_{lit}, and the errors, *RE*, relative to the literature data.

For the cases in which *OF* exceeded the analytical range (Table 2), denoted as $CU_S{}^*$ in Table 5, CU_S was determined using the semi-analytical procedure. As expected from the curve-overlapping behaviour discussed in Fig. 9c, for *OF* values lying in the analytical ranges (Table 2), no differences were observed between CU_S and $CU_S{}^*$ (not reported in Table 5).

Table 5 shows that low *RE* values were obtained, $RE \in [-5.69\,\%, 3.57\,\%]$, except for the cases indicated in bold, where *RE* reaches $-7.70\,\%$. Naturally, high *RE* values could be attributed to discrepancies between experimental *RP-WAR* and the exactly uniform *WAR* assumed in the analytical or semi-analytical procedure.

The data from literature (Li et al., 2015; Li & Kawano, 1996; Pan et al., 2024; Yang et al., 2024) are also plotted in Fig. 9c, where it is possible to observe that the suggested procedure is able to capture the irregular CU_S trend across different *OF* values, described by the theoretical approach.

Unfortunately, equilateral triangular layouts are less common than square layouts, and no data were found. Since the same procedure is adopted for both equilateral triangular and square layouts, it is reasonable to conclude that the proposed approach could be valid for both layouts.

The mean *WAR*, M_S (Eq. (50)), was not verified because the selected studies did not report mean application rates. Nevertheless, mean *WAR* remains a key performance variable, as it controls the irrigation time required to achieve a target average application depth and therefore affects sprinkler irrigation efficiency from an energy-saving perspective, as discussed in Section 4.3.

4.2. Comparison between commonly applied design principles with results from the suggested approach under different layouts and radial patterns

4.2.1. Square layouts

Keller and Bliesner (1990) suggested optimal sprinkler spacing, *S*, expressed as a percentage of wetted diameter, 2 *WR*, expected to provide acceptable application uniformities for different *RPs-WAR* and for both square and equilateral triangular layouts. For square layouts, these

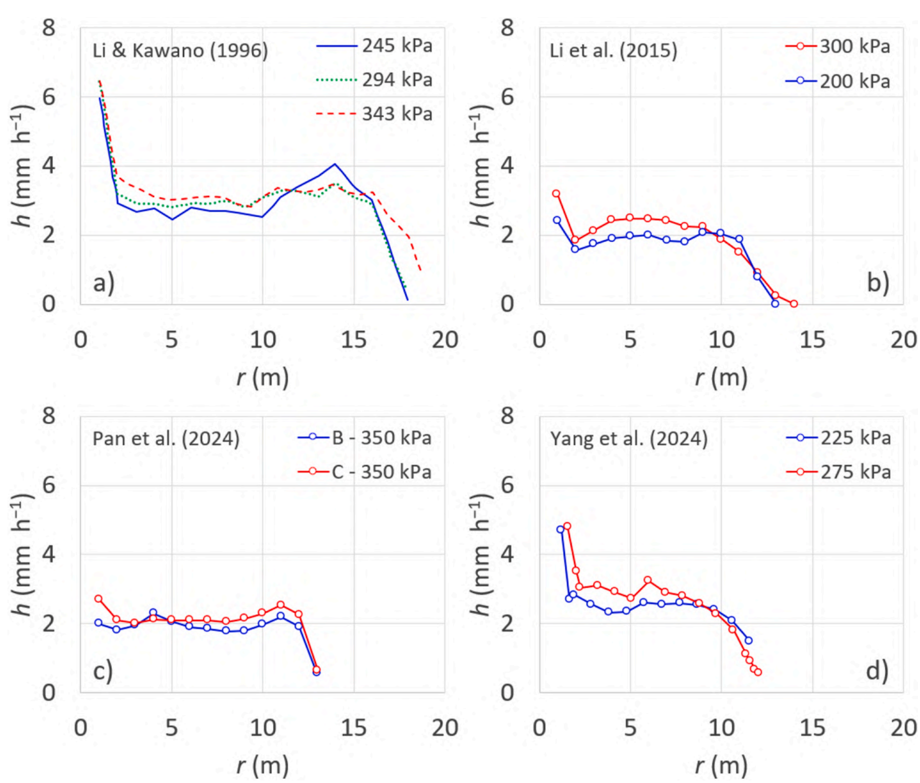

Fig. 11. Radial pattern of water application rate of individual sprinklers under different operating pressure, provided by a) Li and Kawano (1996), b) Li et al. (2015), d) Yang et al. (2024), and c) by varying diffuser tooth length, at the same operating pressure (Pan et al., 2024).

Table 4
Operating pressure head, P, wetted radius, WR, square sprinkler spacing, S, the corresponding overlap fraction, OF, the OF range allowing analytical solution to be selected, and the values of S[a], for literature data from Li and Kawano (1996), Li et al. (2015), Pan et al. (2024), and Yang et al. (2024).

References	P (kPa)	WR (m)	Square sprinkler spacing, $S \times S$ (m)	OF (Eq. (3))	OF range	S[a] (Eq. (4))
Li and Kawano (1996)	245	17.9	18 × 18 m	0.497	[0.488, 0.5]	1.006
	294	18.7	18 × 18 m	0.519[a]	–	0.962
	343	18.9	18 × 18 m	0.524[a]	–	0.952
	392	19.5	18 × 18 m	0.538[a]	–	0.924
Li et al. (2015)	200	13.0	14 × 14 m	0.462	[0.373, 0.488]	1.076
	300	14.0	14 × 14 m	0.500	[0.488, 0.5]	1.000
Pan et al. (2024)	B – 350	13.0	13 × 13 m	0.500	[0.488, 0.5]	1.000
	C – 350	13.0	13 × 13 m	0.500	[0.488, 0.5]	1.000
	B – 350	13.0	14.3 × 14.3 m	0.450	[0.373, 0.488]	1.100
	C – 350	13.0	14.3 × 14.3 m	0.450	[0.373, 0.488]	1.100
	B – 350	13.0	15.6 × 15.6 m	0.400	[0.373, 0.488]	1.200
	C – 350	13.0	15.6 × 15.6 m	0.400	[0.373, 0.488]	1.200
	B – 350	13.0	16.9 × 16.9 m	0.350	[0.293, 0.373]	1.300
	C – 350	13.0	16.9 × 16.9 m	0.350	[0.293, 0.373]	1.300
	B – 350	13.0	18.2 × 18.2 m	0.300	[0.293, 0.373]	1.400
	C – 350	13.0	18.2 × 18.2 m	0.300	[0.293, 0.373]	1.400
Yang et al. (2024)	225	11.5	10 × 10 m	0.565[a]	–	0.870
	275	12	10 × 10 m	0.583[a]	–	0.834
	225	11.5	12 × 12 m	0.478	[0.373, 0.488]	1.044
	275	12	12 × 12 m	0.500	[0.488, 0.5]	1.000

[a] For $OF > 0.5$, CU_S was calculated numerically.

recommended S are reported in Table 6, together with the corresponding values of S_* and OF adopted in the proposed procedure. These parameters allow Keller and Bliesner (1990) recommended configurations to be reproduced and assessed quantitatively, enabling the expected acceptable application uniformities to be verified in terms of CU_S, which was not explicitly reported in their study.

The resulting CU_S reported in Table 6 confirms that the configurations recommended by Keller and Bliesner (1990) provide good application uniformities, with $80\,\% < CU_S < 90\,\%$, for the uniform and concave *RPs-WAR*, and excellent application uniformity, with $CU_S > 90\,\%$, for the convex and linear *RPs-WAR*, according to the CU_S classification ranges proposed by Andrade et al. (2022). However, it should be noted that the concave *RP-WAR* considered was selected using $\alpha = 1$, which produced a particularly pronounced concavity, whereas Keller and Bliesner (1990) provided only a qualitative description of *RP-WAR*.

Fig. 12a–d illustrates the results in terms of the spatial distribution of *WAR*. For the uniform *RP-WAR*, the values of CU_S were obtained through the suggested procedure, whereas for the parabolic *RPs-WAR*, they were obtained using the numerical approach of Baiamonte and Vaccaro (2026).

The lowest CU_S value, obtained for the concave *RP-WAR* (Fig. 12d), is likely attributable to the imposed $\alpha = 1$, which produces low values of *WAR* in the peripheral portion of the wetted area, despite the overlap among wetted circles. Contrarily, the uniform *RP-WAR* (Fig. 12a) produces higher values of *WAR* within the overlapped areas, resulting in $CU_S = 86.2\,\%$, which is lower than those obtained for both the convex (Fig. 12b) and linear (Fig. 12c) *RPs-WAR*.

The results of the applications performed using OF values required to achieve $CU_S = 90\,\%$ are shown in Fig. 13a–d. Compared with the S_* recommended by Keller and Bliesner (1990), Fig. 13a–d shows that for convex (Fig. 13b) and linear (Fig. 13c) *RPs-WAR*, excellent application uniformities ($CU_S \approx 90\,\%$) can be achieved for higher S_* values (i.e.,

Table 6
Sprinkler spacing recommended by Keller and Bliesner (1990), together with the corresponding parameters derived using the uniform *RP-WAR* assumption and the numerical procedure (Baiamonte & Vaccaro, 2026), for square layout, under different *RP-WAR* conditions.

RP-WAR	Sprinkler spacing, S (Keller & Bliesner, 1990)	α	S_*	OF	CU_S	OF (for $CU_S = 90\,\%$)
uniform	2 WR × 40 %	–	2 × 0.4	0.60	86.22	0.546
convex	2 WR × 60 %	−1	2 × 0.6	0.40	92.77	0.363
linear	2 WR × 55 %	0	2 × 0.55	0.45	97.38	0.397
concave	2 WR × 50 %	1	2 ×0.5	0.50	81.58	0.562

Table 5
Parameters to apply the analytical procedure for literature data from Li and Kawano (1996), Li et al. (2015), Pan et al. (2024), and Yang et al. (2024).

References	P (kPa)	a	m (Eq. (14))	n (Eq. (14))	$\Psi_{s,1}$ (Eq. (26))	$\Psi_{s,2}$ (Eq. (27))	CU_S (%)	CU_S[a] (%)	CU_{lit} (%)	RE (%)
Li and Kawano (1996)	245	0.503	0.864	0.703	0.006	0.527	82.54	–	82.00	−0.66
	294	0.481	0.877	0.733	−0.037	0.502	–	83.32	83.70	0.46
	343	0.476	0.879	0.739	−0.047	0.496	–	83.81	83.90	0.10
	392	0.462	0.887	0.758	−0.074	0.480	–	87.11	89.90	3.20
Li et al. (2015)	200	0.538	0.843	0.648	0.080	0.569	74.75	–	73.27	−1.97
	300	0.500	0.866	0.707	0.000	0.524	82.78	–	81.11	−2.01
Pan et al. (2024)	B – 350	0.500	0.866	0.707	0.000	0.524	82.78	–	76.40	**−7.70**
	C – 350	0.500	0.866	0.707	0.000	0.524	82.78	–	76.70	**−7.34**
	B – 350	0.550	0.835	0.628	0.106	0.582	73.38	–	76.00	3.57
	C – 350	0.550	0.835	0.628	0.106	0.582	73.38	–	74.80	1.94
	B – 350	0.600	0.800	0.529	0.228	0.644	76.36	–	78.30	2.55
	C – 350	0.600	0.800	0.529	0.228	0.644	76.36	–	76.90	0.71
	B – 350	0.650	0.760	0.394	0.381	0.708	77.61	–	73.20	−5.69
	C – 350	0.650	0.760	0.394	0.381	0.708	77.61	–	72.30	**−6.85**
	B – 350	0.700	0.714	0.141	0.644	0.775	69.83	–	66.80	−4.35
	C – 350	0.700	0.714	0.141	0.644	0.775	69.83	–	64.60	**−7.50**
Yang et al. (2024)	225	0.435	0.901	0.789	−0.123	0.450	–	92.67	88.73	−4.25
	275	0.417	0.909	0.808	−0.155	0.430	–	87.24	87.16	−0.09
	225	0.522	0.853	0.675	0.044	0.549	78.56	–	76.02	−3.23
	275	0.500	0.866	0.707	0.000	0.524	82.78	–	79.88	−3.50

[a] CU calculated from the semi-analytical solution, CU_S*. Bold RE values refer to high values of REs.

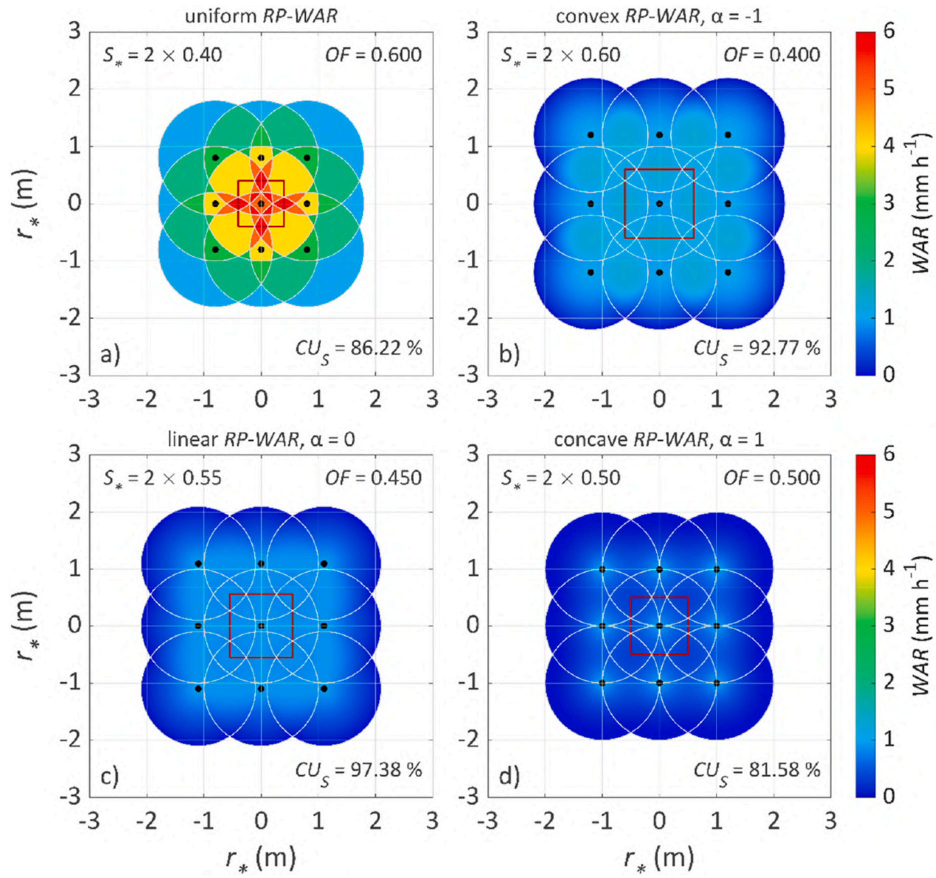

Fig. 12. Spatial distribution of *WAR* for sprinkler spacing recommended by Keller and Bliesner (1990), for a) uniform, b) convex (α = −1), c) linear (α = 0), and d) convex (α = 1) *RP-WAR*, and square layouts.

lower *OF* values, see Table 6), thus reducing the required number of sprinklers and the associated investment costs.

More importantly, the abovementioned drawbacks (CU_S < 90 %) for the uniform (Fig. 12a) *RP-WAR* under the Keller and Bliesner (1990) configuration are mitigated by a higher S_* (i.e., lower *OF*, Fig. 13a).

4.2.2. Equilateral triangular layouts

For equilateral triangular layouts, the CU_H values reported in Table 7 show that the *S* recommended by Keller and Bliesner (1990) provide markedly different application uniformities depending on the *RP-WAR*.

Good application uniformity was obtained for the concave *RP-WAR*, with CU_H = 87.83 %, whereas excellent application uniformities were achieved for the convex and linear *RPs-WAR*, with CU_H values of 90.89 % and 94.02 %, respectively (Andrade et al., 2022). Conversely, the uniform *RP-WAR* resulted in a considerably lower CU_H value of 68.47 %, indicating that the *S* suggested by Keller and Bliesner (1990) is not sufficient to ensure acceptable uniformity (CU_H > 80 %) for this *RP-WAR* under equilateral triangular layouts, at least from the perspective of the suggested approach.

Fig. 14a–d illustrates the spatial distributions of *WAR* for equilateral triangular layouts using the sprinkler spacing recommended by Keller and Bliesner (1990). The low values of CU_H obtained for the uniform *RP-WAR* (Fig. 14a) are mainly ascribed to the relatively low *OF* = 0.30, which produces high *WAR*s in the peripheral overlapped areas within the hexagon reference area, despite the uniform *RP-WAR*.

In contrast, the convex and linear *RPs-WAR* (Fig. 14b and c) show smoother *WAR* distributions within the reference area, resulting in excellent CU_H values. For the concave *RP-WAR* (Fig. 14d), the lower *WAR* values in the peripheral areas, caused by the imposed α = 1, are partly compensated by the larger overlap associated with *OF* = 0.50, but also by the equilateral triangular configuration, leading to a nearly excellent *WAR* uniformity.

Results using *OF* values for $CU_H \approx$ 90 % are shown in Fig. 15a–d. For the uniform *RP-WAR* (Fig. 15a), the target $CU_H \approx$ 90 % required a substantial increase in *OF*, from 0.30 to 0.441, thus deviating from the recommendations of Keller and Bliesner (1990).

Conversely, for the convex (Fig. 15b) and linear (Fig. 15c) *RPs-WAR*, $CU_H \approx$ 90 % was achieved with lower *OF* values than those suggested by Keller and Bliesner (1990), decreasing from 0.350 to 0.242 and from 0.340 to 0.308, respectively. This indicates that acceptable application uniformity can be maintained with wider sprinkler spacing, thereby reducing the number of sprinklers and associated investment costs. For the concave *RP-WAR* (Fig. 15d), the *OF* required to reach $CU_H \approx$ 90 % was only slightly higher than the recommended value, confirming the suitability of the authors' guideline for this configuration.

It is important to note that, although a uniform *RP-WAR* may appear attractive for achieving a highly uniform *WAR* distribution, the results presented above for both square and equilateral triangular layouts (Fig. 13a and 15a) show that it is less favourable than convex and linear *RPs-WAR*. This is because uniform *RP-WAR* requires high *OF* values to compensate for the elevated *WAR* values occurring in the peripheral regions where the wetted circles overlap. Moreover, high *OF* values correspond to low S_* values, implying a greater number of sprinklers. Therefore, from an investment-cost perspective, uniform *RP-WAR* is not recommended, as it necessitates the installation of more sprinklers.

4.3. Performance of square and equilateral triangular layouts with uniform and parabolic RPs-WAR

Under uniform *RP-WAR*, for square and equilateral triangular

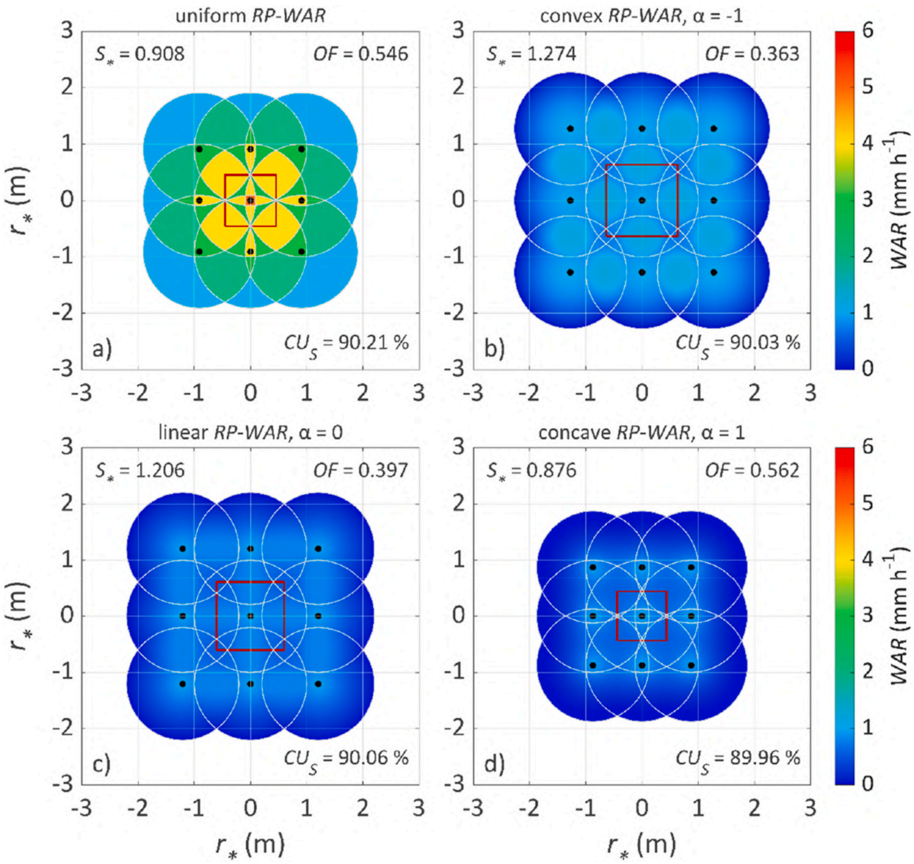

Fig. 13. Spatial distribution of *WAR* for sprinkler spacing determined by the suggested procedure, for uniform *RP-WAR*, and by the numerical one by Baiamonte and Vaccaro (2026), to achieve $CU_S = 90\,\%$, for a) uniform, b) convex ($\alpha = -1$), c) linear ($\alpha = 0$), and d) convex ($\alpha = 1$) *RP-WAR*, and square layouts.

Table 7
Sprinkler spacing recommended by Keller and Bliesner (1990), together with the corresponding parameters derived using the uniform *RP-WAR* assumption and the numerical procedure (Baiamonte & Vaccaro, 2026), for equilateral triangular layout, under different *RP-WAR* configurations.

RP-WAR	Sprinkler spacing, *S* (Keller & Bliesner, 1990)	α	S_*	*OF*	CU_H	*OF* (for $CU_H = 90\,\%$)
Uniform	2 *WR* × 70 %	–	2 × 0.7	0.30	68.47	0.441
Convex	2 *WR* × 65 %	−1	2 × 0.65	0.35	90.89	0.242
Linear	2 *WR* × 66 %	0	2 × 0.66	0.34	94.02	0.308
Concave	2 *WR* × 50 %	1	2 × 0.5	0.50	87.83	0.508

layouts, Fig. 16 plots the mean, *M* (Fig. 16a), the coefficient of variation, *CV* (Fig. 16b), and the Christiansen uniformity coefficient, *CU* (Fig. 16c), versus *OF*. The *OF* values that need to achieve high *CU* (*CU* = 85, 90 and 95 %), already presented in Table 3, are also indicated.

For equilateral triangular layouts, Fig. 16c also plots the $CU = 90\,\%$ value, obtained at a very low $OF = 0.034$. As previously observed, although this would be economically attractive due to its low sprinkler density, it must be rejected because it does not ensure full coverage ($OF < 0.134$; see Table 1).

The comparison displayed in Fig. 16 shows a strong sensitivity of sprinkler performance to *OF* values. At $CU = 95\,\%$, equilateral triangular layouts require a higher *OF* (i.e., a lower S_*, Eq. (4)), indicating a higher sprinkler density; however, the corresponding higher mean *WAR* (red dot, Fig. 16a) suggests substantial energy savings, which may partially offset this disadvantage depending on local energy costs and the target irrigation depth.

The selection of a target *CU* should also be interpreted in relation to crop response rather than as a purely hydraulic criterion. Crop-specific studies indicate that the effect of *WAR* uniformity on yield can vary markedly with crop sensitivity, irrigation depth, climate and soil-water redistribution.

For example, studies on alfalfa (Montazar & Sadeghi, 2008), winter wheat (Li & Rao, 2003), barley (Abd El-Wahed et al., 2016), and maize (Dechmi et al., 2003; Mantovani et al., 1995) generally support the relevance of improving *WAR* uniformity to reduce crop yield variability, increase water use efficiency, and optimise the applied irrigation amount.

However, the target *CU* level is not universal. In particular, Mateos et al. (1997) showed that cotton yield was not significantly affected by a reduction in *WAR* uniformity, because of the curvilinear yield response and the damping effect of soil-water redistribution. Therefore, for crops such as cotton, lower *CU* values may be agronomically acceptable under specific soil and climatic conditions, whereas crops more sensitive to *WAR* uniformity or arid environments may justify adopting higher *CU* targets, close to 90 %.

In addition to crop response, the mean *WAR*, *M*, associated with a given *OF* and sprinkler layout must be compatible with the soil hydraulic properties. Therefore, the design objective is not only to achieve high application uniformity but also to ensure that the applied water infiltrates the soil and remains available within the root zone. This requirement is particularly important because high water application rates and droplet kinetic energy can promote surface sealing, reduce infiltration, and increase the risks of runoff, deep percolation, and soil erosion.

Previous studies have shown that these processes are strongly controlled by soil texture, antecedent water content, application rate, and droplet kinetic energy, while slope conditions may further increase runoff and erosion risks in sloping fields (AL-Kayssi & Mustafa, 2016;

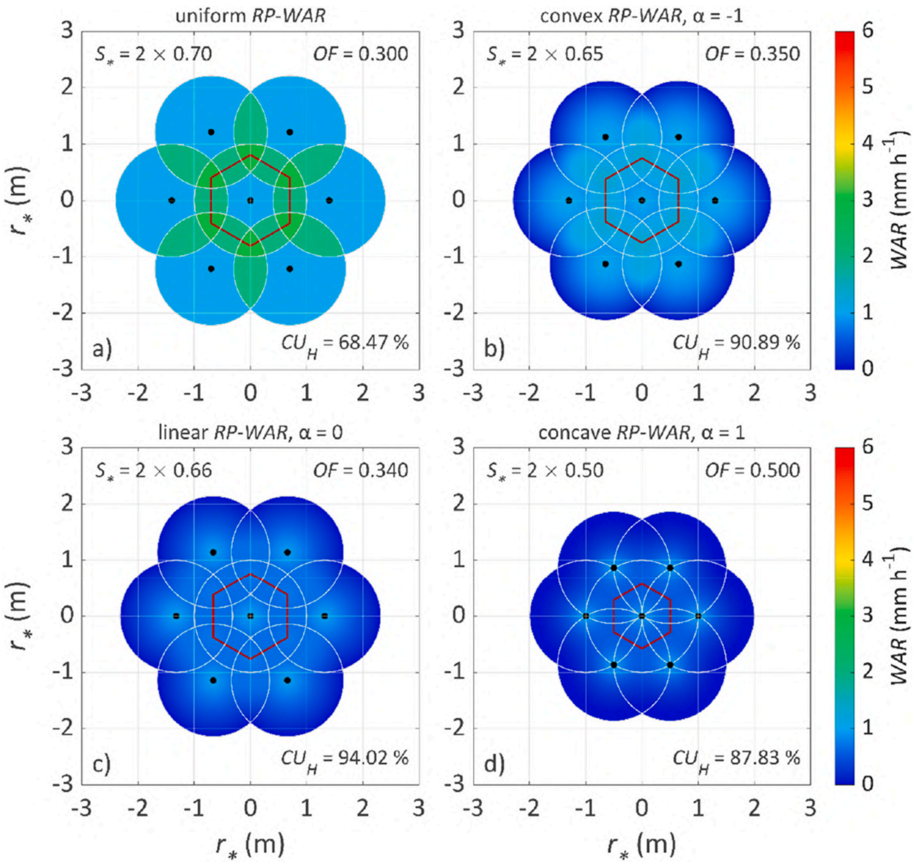

Fig. 14. Spatial distribution of *WAR*, for sprinkler spacing recommended by Keller and Bliesner (1990), for a) uniform, b) convex (α = −1), c) linear (α = 0), and d) convex (α = 1) *RP-WAR*, and equilateral triangular layouts.

Chen, Li, Wang, & Song, 2023, Chen, Li, Wang, & Song, 2023; Lehrsch & Kincaid, 2010; Lu et al., 2019; Santos et al., 2003). Consequently, the *OF*, corresponding S_*, and *M* values derived in this study should be interpreted as hydraulic-uniformity design criteria for level-field conditions and subsequently verified against site-specific crop requirements and soil infiltration capacity.

The results presented in Section 4.2 confirm that both *RP-WAR* and sprinkler layouts strongly influence mean *WAR* and *WAR* uniformity. However, achieving a target *CU* does not uniquely determine the performance of the sprinkler irrigation system, since the associated mean *WAR*, and hence the irrigation time required to deliver a target depth, also varies with layouts and *RP-WAR*.

The trade-off between sprinkler density and energy demand has received limited attention in the literature and is investigated herein. To this end, two efficiency indices are introduced to classify sprinkler system performance according to i) target *CU* levels (90 % and 95 %), ii) sprinkler layouts (square or equilateral triangular), and iii) *RP-WAR*, including the uniform pattern examined in this study, and convex, linear, and concave *RPs-WAR*, according to Baiamonte and Vaccaro (2026).

4.3.1. *Efficiency indices*

Two efficiency indices were denoted: EI_{SP}, related to the required number of sprinklers, and EI_{EN}, related to the energy saving. These two indices exactly coincide with the *RA* and with the weighted mean, *M*, respectively:

$$EI_{SP} \equiv RA \tag{65}$$

$$EI_{EN} \equiv M \tag{66}$$

To enable a consistent comparison among configurations, EI_{SP} and EI_{EN} were normalised as follows:

$$EI_{SP*} = \frac{EI_{SP} - EI_{SPmin}}{EI_{SPmax} - EI_{SPmin}} \tag{67}$$

$$EI_{EN*} = \frac{EI_{EN} - EI_{ENmin}}{EI_{ENmax} - EI_{ENmin}} \tag{68}$$

where EI_{SPmax}, EI_{ENmax}, EI_{SPmin} and EI_{ENmin} are the corresponding maximum and minimum values of the entire $CU = 95\ \%$ and $90\ \%$ dataset.

For $CU = 95\ \%$ and $90\ \%$, Table 8 and Table 9 report the geometrical solid-set sprinkler parameters, under uniform *RP-WAR* (Table 3), and under convex, linear and concave *RPs-WAR* provided by Baiamonte and Vaccaro (2026, see Table 3), together with the efficiency indices not normalised (Eqs. (65) and (66)) and normalised (Eqs. (67) and (68)).

4.3.2. *Sprinkler layouts and RPs-WAR ranking*

First, a weighted aggregation (single-index) approach was applied, in which the overall efficiency index, *EI*, is defined as follows:

$$EI = w_{SP}\, EI_{SP*} + w_{EN}\, EI_{EN*} \tag{69}$$

where w_{SP} and w_{EN} are the weights to be attributed to the number of sprinklers and energy efficiency normalised indices, respectively, describing their importance in decision-making, and depending on energy and/or sprinkler costs ($w_{SP} + w_{EN} = 1$).

For $CU = 95\ \%$ and $90\ \%$, Fig. 17a–c and Fig. 17e–f plot the results obtained by applying the single-index approach, assuming $w_{SP} = 0.5$ (equal weights), $w_{SP} = 0.3$ and 0.7, respectively. Since higher index values indicate better solid-set sprinkler system performance, the ranking was assigned in descending order.

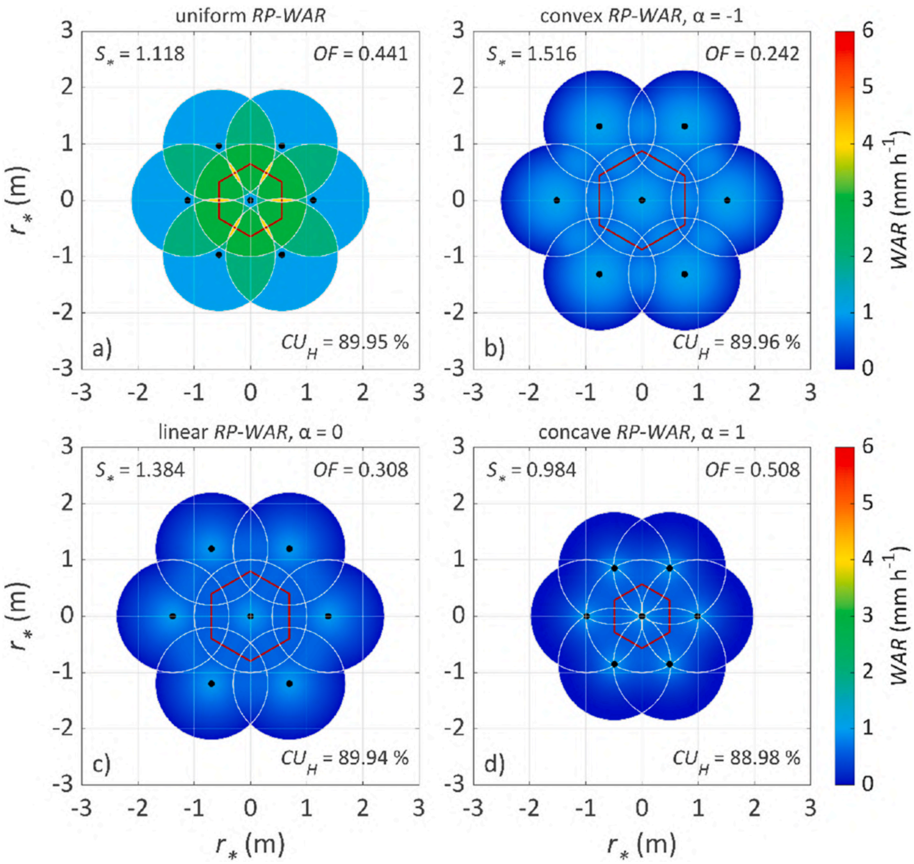

Fig. 15. Spatial distribution of *WAR*, for sprinkler spacing determined by the suggested procedure, for uniform *RP-WAR*, and by the numerical one by Baiamonte and Vaccaro (2026), to achieve $CU_H = 90\,\%$, for a) uniform, b) convex ($\alpha = -1$), c) linear ($\alpha = 0$), and d) convex ($\alpha = 1$) *RP-WAR*, and equilateral triangular layouts.

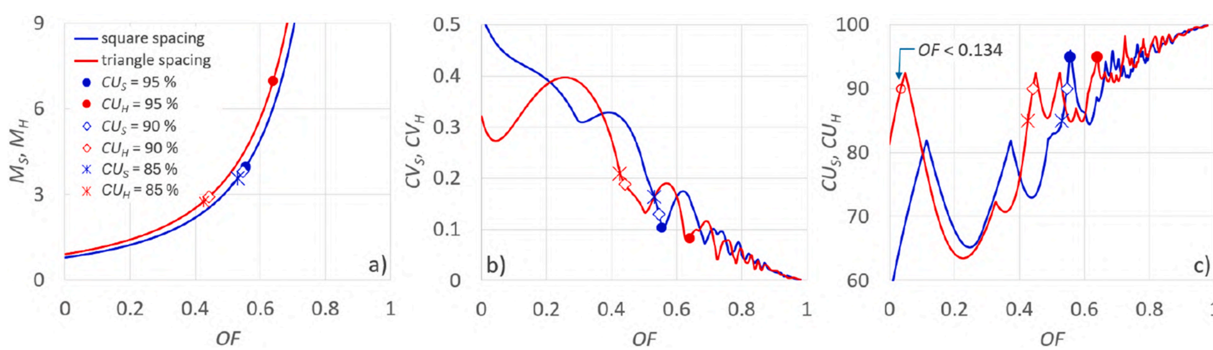

Fig. 16. Comparison between a) mean *WAR*, *M* (mm h^{-1}), b) coefficient of variation, *CV*, and c) Christiansen uniformity coefficient, *CU*, versus *OF*, of square and equilateral triangular layouts. The *OF* values corresponding to $CU = 90\,\%$ and 95 % are indicated (see Table 2).

Fig. 17 shows that, for any of the three assumed weights, in general convex *RPs-WAR* ($\alpha < 0$) provide a better performance, especially for equilateral triangular layouts (H), which could be attributed to the higher *WAR* occurring at the peripheral radial patterns, compared to concave or linear *RPs-WAR*.

As it could be expected, for $w_{SP} = 0.3$ i.e. $w_{EN} = 0.7$, when a greater importance is given to the energy costs, uniform *RPs-WAR* show the best performance, for both $CU = 95$ and 90 %, and square (S) and equilateral triangular layouts (H). This is because of the corresponding very high mean values, i.e. EI_{EN} values (Table 8 andTable 9), which characterise uniform *RP-WAR*, preventing long irrigation times, thus saving a lot of energy. When $w_{SP} = 0.7$ is assumed, the uniform *RPs-WAR* are surpassed by convex *RPs-WAR*, since a higher importance is given to the sprinkler costs.

In conclusion, results are reasonable and may help provide decision-making in solid-set sprinkler irrigation system design. However, the weighted aggregation (single-index) approach requires choosing weights, which are often subjective, especially when sprinklers and energy cost data are not available, difficult to justify, and can strongly bias the results, collapsing multiple factors into one single index that can significantly influence or distort the outcomes.

Towards the aim to preserve information, avoid arbitrary weight assumptions, and provide a richer and more robust framework for analysing the sprinkler performance, the Pareto-ranking method as a multi-criteria decision-making, was also applied.

For each uniformity target ($CU = 90\,\%$ and $CU = 95\,\%$), the *RPs-WAR* alternatives (convex, linear, concave and uniform) and the two layouts (square and equilateral triangular layouts) were ranked using

Table 8
For $CU = 95$ %, *ID* code associated with convex/linear/concave/uniform shape of the *RP-WAR*, corresponding geometrical parameters of the sprinklers solid-set, and efficiency indexed not normalised (EI_{SP}, EI_{EN}) and normalised (EI_{SP*}, EI_{EN*}).

ID	*RP-WAR*	α	*CU* (%)	*OF*	S_*	*a*	$EI_{SP} \equiv RA$	EI_{SP*}	$EI_{EN} \equiv M$	EI_{EN*}
−α1(S)	*convex*	−1	94	0.419	1.162	0.581	1.350	0.705	1.162	0.076
−α0.8(S)		−0.8	94	0.424	1.152	0.576	1.327	0.687	1.103	0.067
−α0.6(S)		−0.6	95	0.416	1.168	0.584	1.364	0.716	0.996	0.050
−α0.4(S)		−0.4	95	0.414	1.172	0.586	1.374	0.723	0.914	0.037
−α0.2(S)		−0.2	95	0.42	1.16	0.58	1.346	0.701	0.855	0.028
α0(S)	*linear*	0	95	0.431	1.138	0.569	1.295	0.662	0.807	0.020
α0.2(S)	*concave*	0.2	95	0.45	1.1	0.55	1.210	0.595	0.778	0.015
α0.4(S)		0.4	95	0.483	1.034	0.517	1.069	0.484	0.782	0.016
α0.6(S)		0.6	95	0.531	0.938	0.469	0.880	0.336	0.833	0.024
α0.8(S)		0.8	95	0.583	0.834	0.417	0.696	0.191	0.907	0.036
α1(S)		1	95	0.631	0.738	0.369	0.545	0.073	0.961	0.044
UNIF(S)	*uniform*	–	95	0.555	0.890	0.445	0.792	0.267	3.965	0.523
−α1(H)	*convex*	−1	95	0.294	1.412	0.706	1.727	1	0.909	0.036
−α0.8(H)		−0.8	95	0.305	1.39	0.695	1.673	0.958	0.876	0.031
−α0.6(H)		−0.6	95	0.319	1.362	0.681	1.607	0.906	0.847	0.026
−α0.4(H)		−0.4	95	0.325	1.35	0.675	1.578	0.884	0.796	0.018
−α0.2(H)		−0.2	95	0.335	1.33	0.665	1.532	0.847	0.752	0.011
α0(H)	*linear*	0	95	0.355	1.29	0.645	1.441	0.776	0.726	0.007
α0.2(H)	*concave*	0.2	95	0.375	1.25	0.625	1.353	0.707	0.696	0.002
α0.4(H)		0.4	95	0.405	1.19	0.595	1.226	0.608	0.682	0
α0.6(H)		0.6	95	0.455	1.09	0.545	1.029	0.453	0.712	0.005
α0.8(H)		0.8	95	0.523	0.954	0.477	0.788	0.264	0.793	0.018
α1(H)		1	95	0.586	0.828	0.414	0.594	0.112	0.88	0.032
UNIF(H)	*uniform*	–	95	0.640	0.720	0.361	0.450	0	6.978	1

Table 9
For $CU = 90$ %, *ID* code associated with convex/linear/concave/uniform shape of the *RP-WAR*, corresponding geometrical parameters of the sprinklers solid-set, and efficiency indexed not normalised (EI_{SP}, EI_{EN}) and normalised (EI_{SP*}, EI_{EN*}).

ID	*RP-WAR*	α	*CU* (%)	*OF*	S_*	*a*	$EI_{SP} \equiv RA$	EI_{SP*}	$EI_{EN} \equiv M$	EI_{EN*}
−α1(S)	*convex*	−1	90	0.363	1.274	0.637	1.623	0.700	0.967	0.162
−α0.8(S)		−0.8	90	0.364	1.272	0.636	1.618	0.696	0.905	0.144
−α0.6(S)		−0.6	90	0.369	1.262	0.631	1.593	0.675	0.854	0.129
−α0.4(S)		−0.4	90	0.375	1.25	0.625	1.563	0.650	0.803	0.114
−α0.2(S)		−0.2	90	0.384	1.232	0.616	1.518	0.614	0.758	0.101
α0(S)	*linear*	0	90	0.397	1.206	0.603	1.454	0.562	0.719	0.089
α0.2(S)	*concave*	0.2	90	0.413	1.174	0.587	1.378	0.500	0.683	0.078
α0.4(S)		0.4	90	0.437	1.126	0.563	1.268	0.409	0.66	0.072
α0.6(S)		0.6	90	0.472	1.056	0.528	1.115	0.284	0.656	0.070
α0.8(S)		0.8	90	0.517	0.966	0.483	0.933	0.136	0.673	0.075
α1(S)		1	90	0.562	0.876	0.438	0.767	0	0.682	0.078
UNIF(S)	*uniform*	–	90	0.546	0.908	0.454	0.824	0.047	3.803	1
−α1(H)	*convex*	−1	90	0.242	1.516	0.758	1.990	1	0.789	0.110
−α0.8(H)		−0.8	90	0.251	1.498	0.749	1.943	0.962	0.754	0.099
−α0.6(H)		−0.6	90	0.261	1.478	0.739	1.892	0.919	0.775	0.106
−α0.4(H)		−0.4	90	0.273	1.454	0.727	1.831	0.870	0.716	0.088
−α0.2(H)		−0.2	90	0.288	1.424	0.712	1.756	0.808	0.656	0.070
α0(H)	*linear*	0	90	0.308	1.384	0.692	1.659	0.729	0.596	0.053
α0.2(H)	*concave*	0.2	90	0.332	1.336	0.668	1.546	0.636	0.537	0.035
α0.4(H)		0.4	90	0.363	1.274	0.637	1.406	0.522	0.477	0.018
α0.6(H)		0.6	90	0.403	1.194	0.597	1.235	0.382	0.417	0
α0.8(H)		0.8	90	0.455	1.09	0.545	1.029	0.214	0.61	0.057
α1(H)		1	90	0.508	0.984	0.492	0.839	0.058	0.624	0.061
UNIF(H)	*uniform*	–	90	0.441	1.118	0.559	1.082	0.258	2.904	0.732

the Pareto method (i.e., non-dominated sorting). The ranking was based only on the two normalised performance indicators, EI_{SP*} and EI_{EN*}, were a value of 1 denotes the highest efficiency and a value of 0 denotes the lowest. Thus, each configuration was represented as a point in the two-objective space (EI_{SP*}; EI_{EN*}). Since both indicators are efficiency measures, both objectives were formulated as maximisation problems.

According to Pareto dominance under maximisation, a solution p_i is said to be dominated by another solution p_j, denoted as $p_j \succ p_i$, if p_j is at least as good as p_i in all objectives and strictly better in at least one objective:

$$p_j \succ p_i \Longleftrightarrow \left[\forall k, p_{j,k} \geq p_{i,k}\right] \bigwedge \left[\exists k : p_{j,k} > p_{i,k}\right] \tag{70}$$

where k denotes the objective index, with $k = 1$ corresponding to EI_{SP*} and $k = 2$ corresponding to EI_{EN*}, and $\succ$ denotes the strict Pareto-dominance relation.

At each iteration, the Pareto method identifies the current Pareto front as the set of all non-dominated solutions among the configurations not yet assigned to a previous front:

$$\mathscr{F}_r = \left\{ i \in P_r : \nexists\, j \in P_r, j \neq i, \text{such that } p_j \succ p_i \right\} \tag{71}$$

where P_r is the set of configurations not yet assigned to a Pareto front at iteration r. Initially, $P_1 = P$, where P is the complete set of configurations. The solutions belonging to F_r are assigned rank r, removed from further comparisons, and the process is repeated on the remaining

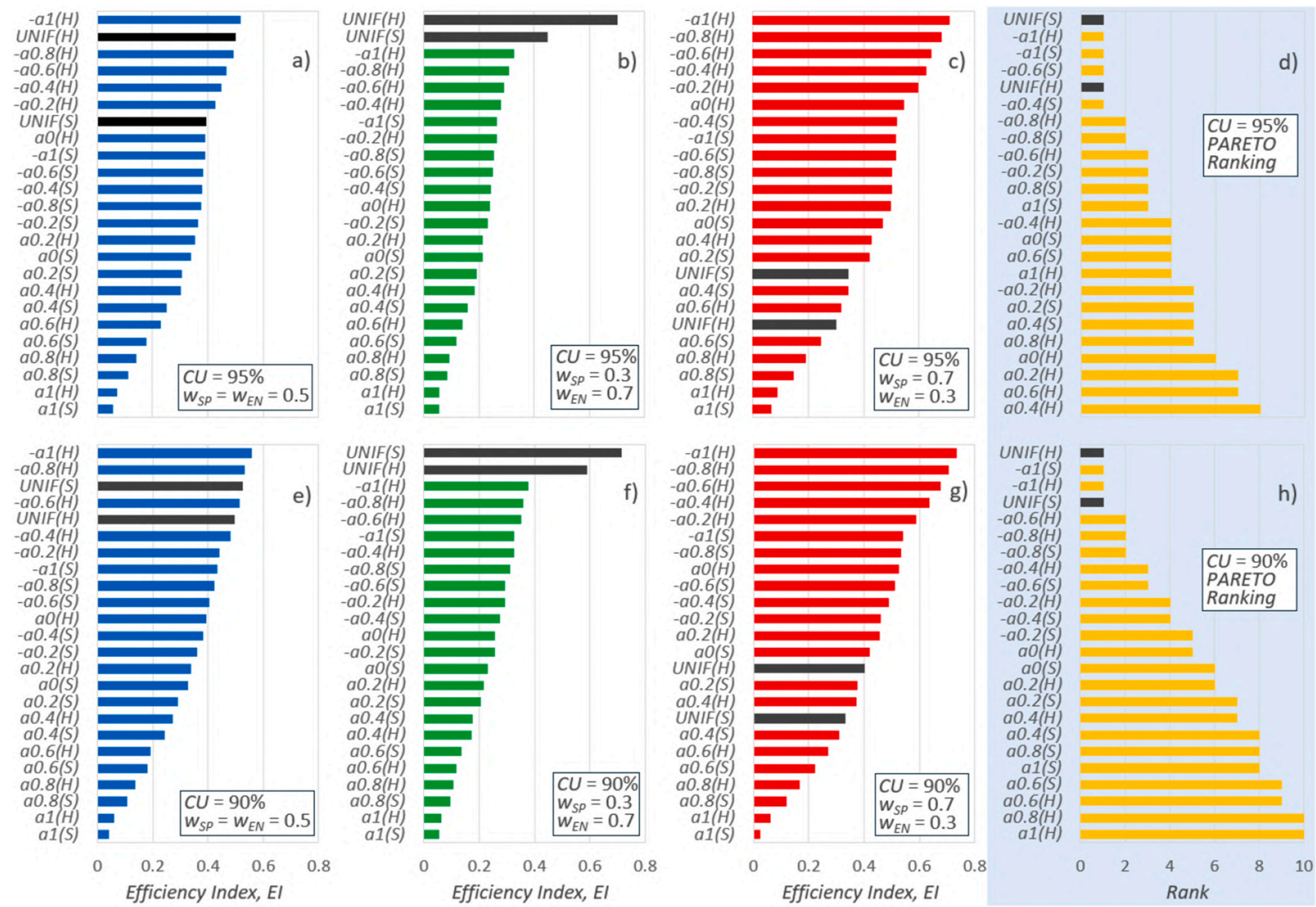

Fig. 17. For $CU = 90\,\%$ (a,b,c) and 95 % (e,f,g) energy efficiency, *EI*, for different radial patterns and sprinkler layouts, by imposing a,e) equal sprinkler and energy weight ($w_{SP} = w_{EN} = 0.5$), b,f) $w_{SP} = 0.3$, and $w_{EN} = 0.7$, and c,g) $w_{SP} = 0.7$, and $w_{EN} = 0.3$. The figure also reports (light blue background) the Pareto ranking d) for $CU = 95\,\%$, and h) for $CU = 90\,\%$.

solutions. This continues until all points are ranked, producing an ordered set of Pareto fronts from best, rank 1, to the worst.

Because configurations within the same front do not dominate one another, a secondary within-front ordering was performed using the Euclidean distance to the ideal point (1,1) in the normalised objective space, $d_i = \sqrt{(1 - EI_{SP*,i})^2 + (1 - EI_{EN*,i})^2}$. Specifically, d_i indicate configurations closer to the ideal simultaneous maximum of both efficiency indicators. The final inter-ranking was therefore obtained by first sorting the configurations according to increasing Pareto rank and then, within each Pareto front, according to increasing Euclidean distance from the ideal point. This distance-based criterion was used only to order configurations within the same front and did not alter the primary Pareto-front classification.

For $CU = 95$ and 90 %, results from Pareto ranking are illustrated in Fig. 17d and h, respectively. The figure shows that the Pareto method provides a convincing ranking of solid-set sprinkler system performance, with the uniform *RP-WAR* among the highest positions and again preferring convex to concave *RPs-WAR*. Such classification is generally recommended, compared to a weighted aggregation (single-index) approach, since the Pareto analysis identifies the entire set of non-dominated solutions, showing all optimal trade-offs between the investigated sprinklers' performance.

Contrarily, if stakeholders' or designers' preferences are clearly known, the weighted aggregation (single-index) approach could be recommended, especially if simplicity and ease in explaining design choices are required, as is usually it is in policy, regulation, and managerial settings.

Overall, the two applied methods to classify solid-set sprinkler performance, according to various *RPs-WAR* and sprinkler layouts, produce consistent and non-contradictory results. Importantly, their combined application offers new insights into the relationships between water application uniformity, return period–based performance indicators, and sprinkler configuration, thereby enhancing the designer's ability to optimise system layout and operational parameters.

However, it must be noted that the presented analysis is purely hydraulic, as it does not account for the fact that the EI_{EN} index, which is related to energy savings and influenced by the mean *WAR* within the reference area, may also depend on other factors such as the soil hydraulic properties and crop water requirements, as discussed in Section 4.3. These factors limit the generality of the obtained *RP-WAR* and sprinkler layouts ranking. In contrast, the EI_{SP} index, which relates to the number of sprinklers required to achieve excellent *CU*, can be considered of more general validity, as it is not influenced by soil or crop characteristics.

In conclusion, the results obtained from the two methods used to rank the potential design solutions are comparable and provide a practical tool to assist designers in selecting the most suitable solution for a given water application rate at the sprinkler location, h_0, because the analysis has been performed in dimensionless terms, as it refers to h_0 equal to 1 mm h^{-1}. When different mean water application rates are required to meet soil and crop water needs, a case-by-case analysis must be performed by varying h_0. The next section presents an application highlighting both the usefulness and the limitations of the efficiency indices defined above.

4.3.3. Case-study application of efficiency indices

The significance of EI_{SP} and EI_{EN} can be made explicit through straightforward dimensional relationships. Since EI_{SP} coincides with the reference area associated with one sprinkler, it is directly related to the number of sprinklers required per unit field area. For a given wetted radius, *WR*, larger values of EI_{SP} correspond to larger sprinkler spacing and therefore to lower sprinkler density. The number of sprinklers per hectare, N_{ha} (N ha^{-1}), can be expressed as:

$$N_{ha} = \frac{10000}{EI_{sp} \times WR^2} \tag{72}$$

Similarly, since EI_{EN} coincides with the dimensionless mean *WAR* over the reference area for $h_0 = 1$ mm h^{-1}, for a sprinkler characterised by a given h_0, the dimensional mean application rate is $M_{dim} = h_0 \times EI_{EN}$ (mm h^{-1}), and the irrigation time required, t_{irr} (h), to deliver a target depth, d_{irr} (mm), is:

$$t_{irr} = \frac{d_{irr}}{M_{dim}} = \frac{d_{irr}}{h_0 \times EI_{EN}} \tag{73}$$

Thus, EI_{EN} is directly related to the operating time required for a given irrigation event. Of course, shorter irrigation times imply lower pumping energy demand. Therefore, the two indices quantify two different engineering objectives: EI_{SP} represents the installation-density component, whereas EI_{EN} represents the operational-energy component.

To illustrate the practical application of the efficiency indices, the experimental *RPs-WAR* of Li et al. (2015), measured at an operating pressure of 200 kPa and characterised by a wetted radius $WR = 13.0$ m, was considered (Figs. 11b and 18). For applied comparison between different *RPs-WAR* (i.e. uniform, convex $\alpha = -1$, linear $\alpha = 0$ and concave $\alpha = 1$) and *WAR* at the sprinkler location, h_0, the mean *WAR*, $\langle h \rangle$, of the measured profile was calculated as the arithmetic mean of the measured values of $h(r)$ along the radial direction, resulting 1.70 mm h^{-1}. This value was set equal for all four configurations to ensure comparison under the same sprinkler discharge conditions (Fig. 18). However, any other *RP–WAR* combination could have been selected for comparison purposes.

The corresponding h_0 values result in 1.70, 2.71, 3.68 and 5.74 mm h^{-1} for the uniform, convex ($\alpha = -1$), linear ($\alpha = 0$), and concave ($\alpha = 1$) patterns, respectively.

For a target $CU = 90$ %, the optimal *OF* and normalised spacing S_* were retrieved from Table 9, and the dimensional spacing $S = S_* \times WR$

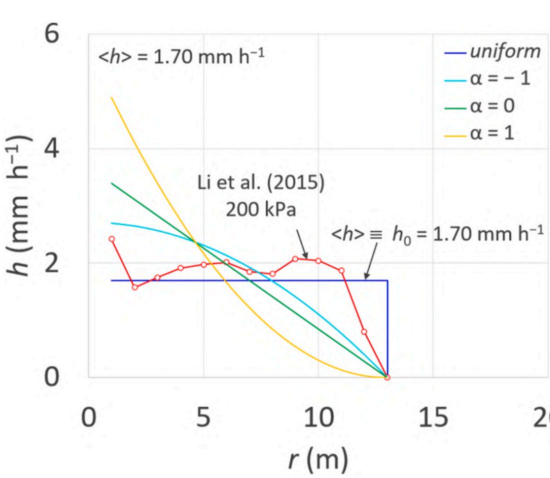

Fig. 18. Uniform, convex ($\alpha = -1$), linear ($\alpha = 0$), and concave ($\alpha = 1$) *RP-WAR*, for the imposed mean *WAR*, $\langle h \geq 1.70$ mm h^{-1}, of experimental data of Li et al. (2015).

was computed. The resulting parameters, together with EI_{SP}, N_{ha}, EI_{EN}, M_{dim}, and t_{irr}, assuming a target irrigation depth $d_{irr} = 10$ mm, are summarised in Table 10 for both square and equilateral triangular layouts.

The results reported in Table 10 reveal two fundamental and conflicting engineering design choices. For square layouts, the convex *RP-WAR* ($\alpha = -1$) minimises installation cost ($N_{ha} = 36$), but requires the longest irrigation time ($t_{irr} = 3.82$ h) to deliver $d_{irr} = 10$ mm. Conversely, the uniform *RP-WAR* delivers the target depth in the shortest time ($t_{irr} = 1.55$ h), albeit at twice the sprinkler density ($N_{ha} = 72$). The same trade-off holds for equilateral triangular layouts, where the convex profile requires $N_{ha} = 30$ at $t_{irr} = 4.68$ h, while the uniform profile increases sprinkler density ($N_{ha} = 55$) but reduces t_{irr} from 4.68 h to 2.03 h. Table 10 also shows that, because the analysis was performed using dimensional quantities (i.e., different values of h_0 and M_{dim}), the Pareto ranking results are not fully consistent with those reported in Fig. 17h. In particular, the linear *RP-WAR*, which had a larger h_0 than the convex and uniform *RPs-WAR* configurations, moved to Rank 1. Concave *RP-WAR* remains the lowest-ranked configuration despite having the highest value of h_0.

The 3D distributions of *WAR* within the respective reference areas and the M_{dim} are illustrated in Fig. 19 (square layouts) and Fig. 20 (equilateral triangular layouts).

For square layouts, the uniform *RP-WAR* (Fig. 19a) produces the most pronounced spatial variability within the reference area, with high *WAR* peaks concentrated at the sprinkler locations and sharp gradients at the reference area boundaries. To achieve $CU = 90$ %, a relatively compact spacing ($S = 11.80$ m, $N_{ha} = 72$) is required. The convex profile ($\alpha = -1$, Fig. 19b) produces a smoother and lower-amplitude *WAR* field, with broad peripheral overlap regions and reduced spatial variability compared with the uniform case; the resulting wider spacing ($S = 16.56$ m) translates into the minimum sprinkler density ($N_{ha} = 36$). The linear ($\alpha = 0$, Fig. 19c) and concave ($\alpha = 1$, Fig. 19d) profiles show progressively greater concentration of water toward the sprinkler location, with the concave profile producing the most pronounced central peak among the parabolic profiles; the latter achieves a reasonable M_{dim} (3.91 mm h^{-1}) but at the cost of the highest sprinkler density among the parabolic profiles ($N_{ha} = 77$).

Analogous behaviour is observed for equilateral triangular layouts (Fig. 20), where the convex configuration achieves the widest spacing ($S = 19.71$ m) and the lowest density ($N_{ha} = 30$), while the uniform profile requires the narrowest spacing ($S = 14.53$ m) but yields the highest M_{dim} (4.94 mm h^{-1}).

It should be noted that the present application was performed at equal mean *WAR*, $\langle h \rangle$ of the isolated sprinkler, and determining different h_0 at the sprinkler location. In practical applications, different sprinklers may have higher or lower h_0 values than those used in this analysis, leading to different application rates and, consequently, different irrigation times. As a result, the relative ranking of the profiles in terms of t_{irr} may change, depending on whether actual commercial sprinklers are characterised by different values of h_0.

In practice, the designer starts from a specific sprinkler characterised by *RP-WAR* and h_0. If the *RP-WAR* is approximately uniform, no shape adjustment is required, and the designer can directly select the *OF* that provides the desired *CU*. Conversely, if the *RP-WAR* is non-uniform, according to Baiamonte and Vaccaro (2026), the corresponding *RP-WAR* allows the optimal *OF* and expected *CU* to be detected. Of course, the configuration to be selected must also account for *CU* crop requirements and the actual mean *WAR*, M_{dim}, which must be consistent with the soil infiltration rate, not contemplated in the normalised approach. Indeed, excessive M_{dim} may require lowering *OF*, possibly at the expense of *CU*, whereas too low M_{dim} may require a sprinkler with a higher h_0.

Once these constraints are defined, the proposed procedure allows the designer to estimate the corresponding t_{irr}, sprinkler density and expected *CU*, and to select the configuration that provides the most

Table 10

For the imposed mean *WAR*, $<h \geq 1.70$ mm h^{-1} of experimental *RP-WAR* data of Li et al. (2015), corresponding geometrical parameters of the sprinklers solid-set, assuming convex ($\alpha = -1$), linear ($\alpha = 0$), concave ($\alpha = 1$), and uniform *RP-WAR*, for square and equilateral triangular layouts. The efficiency indices, EI_{SP} and EI_{EN}, number of sprinklers per hectare, N_{ha}, dimensional mean *WAR*, M_{dim}, the required irrigation time, t_{irr}, and Pareto rank are also reported.

Layouts	*RP-WAR*	h_0 (mm h^{-1})	*WR* (m)	*OF*	S_*	*S* (m)	*CU* (%)	EI_{SP}	N_{ha} (*N* ha^{-1})	EI_{EN}	M_{dim} (mm h^{-1})	t_{irr} (h)	*Pareto Rank*
square	*uniform*	1.70	13.0	0.546	0.908	11.80	90	0.824	72	3.803	6.46	1.55	1
	convex	2.71	13.0	0.363	1.274	16.56	90	1.623	36	0.967	2.62	3.82	1
	linear	3.68	13.0	0.397	1.206	15.68	90	1.454	41	0.719	2.65	3.78	1
	concave	5.74	13.0	0.562	0.876	11.39	90	0.767	77	0.682	3.91	2.55	2
triangular	*uniform*	1.70	13.0	0.441	1.118	14.53	90	1.082	55	2.904	4.93	2.03	1
	convex	2.71	13.0	0.242	1.516	19.71	90	1.990	30	0.789	2.14	4.68	1
	linear	3.68	13.0	0.308	1.384	17.99	90	1.659	36	0.596	2.19	4.56	1
	concave	5.74	13.0	0.508	0.984	12.79	90	0.839	71	0.624	3.58	2.79	2

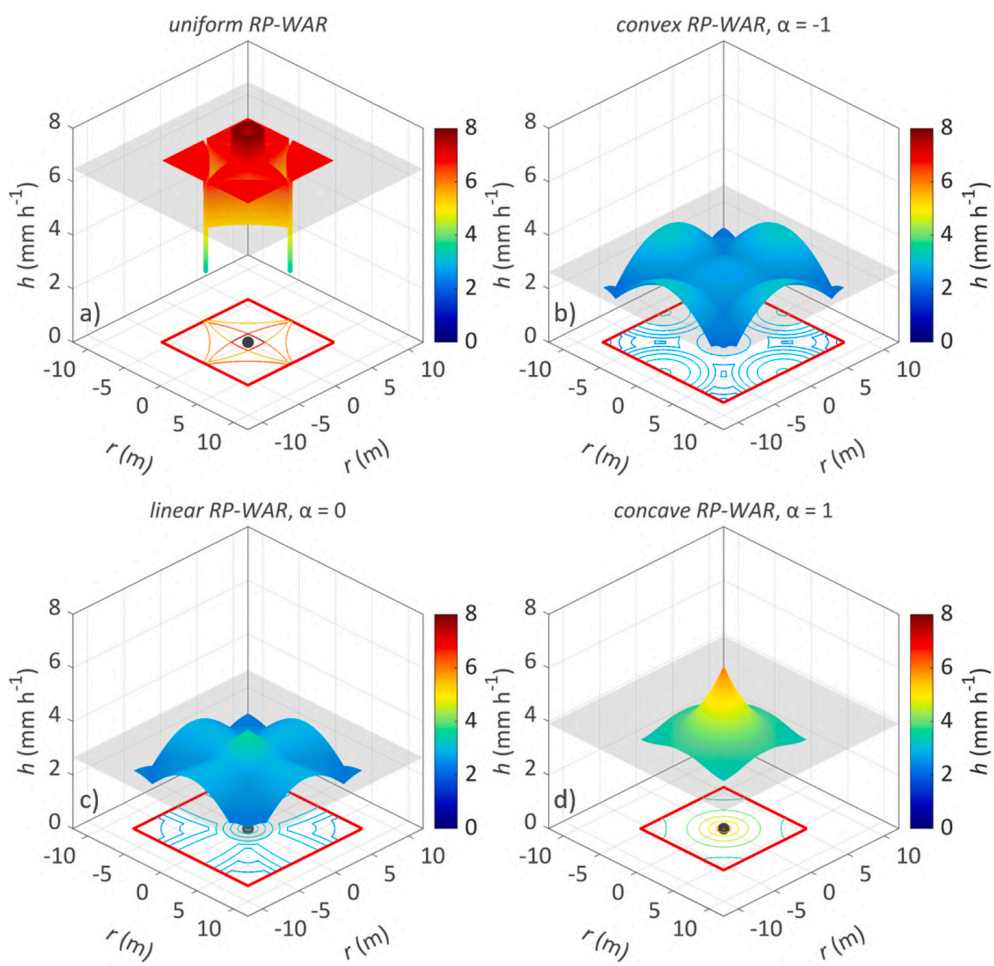

Fig. 19. 3D view of the *WAR* distribution in the reference area, obtained for square spacing, and $CU = 90$ %, for a) uniform, b) convex ($\alpha = -1$), c) linear ($\alpha = 0$), and d) concave ($\alpha = 1$) *RP-WAR*. Grey horizontal planes indicate the dimensional mean *WAR*, M_{dim}.

appropriate compromise among water application rate, irrigation time, *WAR* uniformity and installation cost. The resulting trade-offs can then be assessed using the efficiency indices EI_{SP} and EI_{EN}, which are designed to support decision making.

4.4. Limitations and remarks

The proposed analytical and semi-analytical approach should be interpreted within the assumptions adopted in this study. First, the analytical derivations were developed for an idealised uniform radial precipitation water application rate, *RP-WAR*. Consequently, the derived values of *M*, *CV*, and *CU* depend on the assumed radial application pattern and do not explicitly account for the direct effects of sprinkler design and operating parameters, such as nozzle characteristics, rotational speed, operating pressure, or diffuser configuration. These parameters influence the resulting *RP-WAR* and wetted radius, *WR*, but their explicit relationship with the proposed analytical formulation lies beyond the scope of this study.

Second, the analysis assumes the superposition principle, whereby the application rate of a solid-set sprinkler layout is obtained by summing the contributions of independent sprinklers. As a result, interactions between adjacent sprinkler jets, pressure variability, and local hydraulic disturbances are neglected.

Finally, wind effects were not considered. Because wind modifies both the wetted radius and the radial water application pattern, the calculated *OF*, S_*, *M*, *CV*, and *CU* values are most applicable under low-

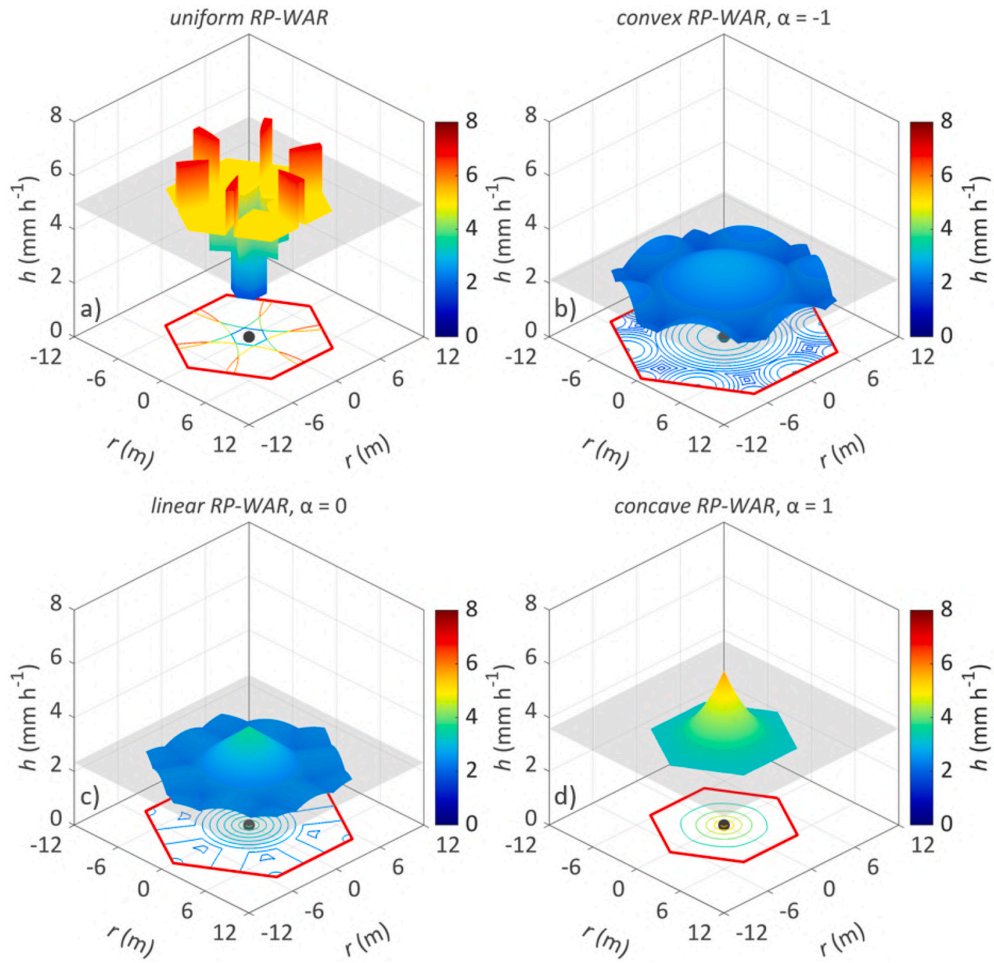

Fig. 20. 3D view of the *WAR* distribution in the reference area, obtained for equilateral triangular layouts, and *CU* = 90 %, for a) uniform, b) convex (α = −1), c) linear (α = 0), and d) concave (α = 1) *RP-WAR*. Grey horizontal planes indicate the dimensional mean *WAR*, M_{dim}.

wind or controlled conditions and should be interpreted with caution under field conditions where wind significantly affects sprinkler performance.

Future research should extend the proposed framework by incorporating measured *RP-WAR* from commercial sprinklers and wind-distorted application patterns. Such developments would enable the influence of sprinkler design, operating conditions, and environmental factors to be explicitly incorporated, thereby broadening the applicability of the proposed methodology under practical field conditions.

5. Conclusions

This study proposes an analytical framework for evaluating sprinkler irrigation uniformity under an idealised uniform radial pattern of water application rate, considering both square and equilateral triangular layouts. The closed-form analytical solutions derived for the partial overlap areas allowed the mean water application rate, *M*, *CV* and Christiansen's uniformity coefficient to be determined within well-defined overlap fraction, *OF*, ranges. These ranges are *OF* ∈ [0.293, 0.5] for square layouts and *OF* ∈ [0.134, 0.422] for equilateral triangular layouts. Within these limits, the analytical and semi-analytical results were in close agreement, confirming the consistency of the proposed analytical formulation. For *CU* targets exceeding 82.84 % and 83.40 % for square and equilateral triangular layouts, respectively, the closed-form analytical solution is no longer applicable, and the semi-analytical solution must be used, since it is the operative design tool over the full *OF* domain.

The proposed procedure was also validated against 20 literature *CU* values, obtaining relative errors ranging from −7.70 % to 3.57 %. This agreement supports the reliability of the proposed approach for estimating sprinkler uniformity under the uniform *RP-WAR* assumption.

The proposed efficiency indices EI_{SP} and EI_{EN} provide a practical basis for quantifying the main design trade-off between sprinkler density and irrigation time. Specifically, EI_{SP} is directly related to sprinkler spacing and density, whereas EI_{EN} is related to the mean application rate and the irrigation time required to apply a target depth. Their combined use through weighted aggregation and Pareto ranking allowed sprinkler configurations to be compared from a multi-criteria perspective. The single-index approach is useful when the relative importance of installation cost and energy saving is known, whereas Pareto ranking identifies non-dominated alternatives without imposing subjective weights.

Overall, no sprinkler layout or *RP-WAR* shape can be considered universally optimal. The most suitable configuration depends on the target *CU*, acceptable sprinkler density, irrigation time, soil infiltration capacity and crop sensitivity to non-uniform water application. Convex *RPs-WAR* are generally advantageous when reducing sprinkler density and installation cost is the main objective, while uniform *RPs-WAR* may be preferable when shorter irrigation times are prioritised.

Under uniform *RP-WAR* and square layouts, the results provided by the suggested procedure are in line with the design indicators suggested by Keller and Bliesner (1990), whereas for equilateral triangular layouts, lower sprinkler spacing is needed to achieve satisfying values of *CU*.

The proposed analytical/semi-analytical framework supports these design decisions by providing a transparent and generalisable method for comparing sprinkler layouts and radial water application patterns.

Data availability section

Data and MATLAB® code are available on request from the corresponding author.

Declaration of generative AI and AI-assisted technologies in the writing process

No generative AI or AI-assisted technologies were used during the preparation of this work.

Funding

This research did not receive any specific grant from funding agencies in the public, commercial, or not-for-profit sectors.

CRediT authorship contribution statement

Giorgio Baiamonte: Conceptualization, Data curation, Formal analysis, Investigation, Methodology, Software, Supervision, Validation, Visualization, Writing – original draft, Writing – review & editing. **Girolamo Vaccaro:** Data curation, Formal analysis, Investigation, Validation, Visualization, Writing – review & editing.

Declaration of competing interest

The authors declare that they have no known competing financial interests or personal relationships that could have appeared to influence the work reported in this paper.

Appendix A

Area A1

The partial area a_1 (Fig. 1b) can be determined by subtracting from the area of the triangle S_1 with base $\overline{II'}$ and height $\overline{OI'}$, the halved circle segment, $S_{seg,1}$, denoted by the central angles towards the points I and I', θ_I and $-\theta_I$, with their difference, $\Delta\theta_I = 2\,\theta_I$:

$$a_1 = S_1 - S_{seg,1} = S_1 - \frac{1}{2}\frac{\Delta\theta_I - sin\Delta\theta_I}{2} \tag{A1}$$

Considering the coordinate of point I (Eq. (17)), S_1 and $\Delta\theta_I$ can be written, respectively:

$$S_1 = \overline{II'} \cdot \overline{OI'} = \frac{1}{2}\left(a - \frac{n}{\sqrt{2}}\right)^2 = \frac{1}{4}\left(1 - 2\sqrt{2}\,a\,n\right) \tag{A2}$$

$$\Delta\theta_I = 2\,arctan\left(\frac{x_I}{2\,a - x_I}\right) = 2\,arctan\left(\frac{\sqrt{2}\,a - n}{\sqrt{2}\,a + n}\right) \tag{A3}$$

Denoting the arctan function $\Psi_{S,1}$ equal to:

$$\Psi_{S,1} = arctan\left(\frac{\sqrt{2}\,a - n}{\sqrt{2}\,a + n}\right) \tag{A4}$$

substituting Eqs. (A2 and A3) into Eq. (A1), and rearranging, the area a_1 and that associated with the reference area, A_1, can be obtained:

$$a_1 = \frac{1}{2}\left[\left(2\,a - \sqrt{2}\,n\right)a - \Psi_{s,1}\right] \tag{A5}$$

$$A_1 = 8\,a_1 = 4\left[\left(2\,a - \sqrt{2}\,n\right)a - \Psi_{S,1}\right] \tag{A6}$$

Area A4

To derive the area a_4, consider the area of the wetted circle centred in $C3(0,0)$, thus assume in this case, the axes origin is in $C3$:

$$x^2 + y^2 = 1 \tag{A7}$$

Making explicit the ordinate, $y = \sqrt{1 - x^2}$, the general vertical segment of the area a_4, $L(x)$, depicted in Fig. 1b, can be expressed as:

$$L(x) = \sqrt{1 - x^2} - a \tag{A8}$$

The analytical solution of the area a_4, can be derived by:

$$a_4 = \frac{1}{2}\int_{-\sqrt{1-a^2}}^{-a} L(x)dx = \frac{1}{2}\int_{-\sqrt{1-a^2}}^{-a}\left(\sqrt{1 - x^2}\right)dx - \frac{1}{2}\int_{-\sqrt{1-a^2}}^{-a} adx \tag{A9}$$

where 1/2 accounts for the extremes of the integral, which refer to the double a_4. Solving the two integrals:

$$\frac{1}{2}\int_{-\sqrt{1-a^2}}^{-a}\left(\sqrt{1-x^2}\right)dx=\frac{1}{4}\left(x\sqrt{1-x^2}+\text{asin}\,x\right)\Big|_{-\sqrt{1-a^2}}^{-a} \tag{A10}$$

$$\frac{a}{2}\int_{-\sqrt{1-a^2}}^{-a}dx=\frac{a}{2}\left(\sqrt{1-a^2}-a\right) \tag{A11}$$

and substituting Eqs. (A10 and A11) into Eq. (A9), provides:

$$a_4=\frac{1}{4}\left(-a\sqrt{1-a^2}-\text{asin}\,a\right)-\left(\frac{1}{4}\left(-a\sqrt{1-a^2}-\text{asin}\sqrt{1-a^2}\right)\right)-\frac{a}{2}\left(\sqrt{1-a^2}-a\right) \tag{A12}$$

Eq. (A12) can be simplified, considering the arctangent properties for $a < 1$, using the m relationship (Eq. (14)), and rearranging:

$$a_4=\frac{1}{2}\left[\Psi_{S,4}-a\,(m-a)\right] \tag{A13}$$

$$A_4=8\,a_4=4\left[\Psi_{S,4}-a\,(m-a)\right] \tag{A14}$$

with $\Psi_{S,4}$ equal to:

$$\Psi_{S,4}=arctan\frac{m-a}{m+a} \tag{A15}$$

Area A3

The analytical solution of the area a_3 can be derived by first calculating the area S_3, denoted as the sum between the polygon whose vertices are described by their coordinates $IAPB$ in the plane, S_{IAPB} (Fig. 1a), and the two segments $\overline{IA}$ and $\overline{IB}$, S_{IA} and S_{IB}, i.e., the regions bounded by a chords $\overline{IA}$ and $\overline{IB}$ and the arcs connecting the chords' endpoints. Since $S_{IA} \equiv S_{IB}$, S_3 is equal to:

$$S_3=S_{IAPB}+2\,S_{IA} \tag{A16}$$

This is because of, once S_3 is known, a_3 can be derived by considering the already derived a_4 (Eq. (A13)):

$$a_3=\frac{S_3}{2}-a_4 \tag{A17}$$

Knowledge of the coordinates of points I, A, and B (Eqs. (17), (19) and (20)) allows the distances $\overline{AB}$ and $\overline{IP}$, and the corresponding area, S_{IAPB}, to be determined, respectively:

$$\overline{AB}=\sqrt{(2a-m-a)^2+(a-(2a-m))^2} \tag{A18}$$

$$\overline{IP}=\sqrt{\left(a-\left(\frac{n}{\sqrt{2}}-a\right)\right)^2+\left(a-\left(\frac{n}{\sqrt{2}}-a\right)\right)^2} \tag{A19}$$

$$S_{IAPB}=\frac{\overline{AB}\cdot\overline{IP}}{2} \tag{A20}$$

Substituting Eqs. (A18 and A19) into Eq. (A20) and rearranging, provides a simple S_{IAPB} relationship, as a function of m and n (Eq. (14)):

$$S_{IAPB}=\frac{n\sqrt{2}\,(m-a)}{2} \tag{A21}$$

To derive S_{IA}, for the circle C6 centred in (2a, 0), the central angles measured in radians towards the points A and I must be considered, respectively:

$$\theta_A=arctan\left(\frac{a}{2a-x_A}\right)=arctan\left(\frac{a}{2a-(2a-m)}\right)=arctan\left(\frac{a}{m}\right) \tag{A22}$$

$$\theta_I=arctan\left(\frac{y_I}{2a-x_I}\right)=arctan\left(\frac{\sqrt{2}\,a-n}{\sqrt{2}\,a+n}\right)=\Psi_{s,1} \tag{A23}$$

Setting:

$$\Psi_{S,2}=arctan\left(\frac{a}{m}\right) \tag{A24}$$

and denoting $\Delta\theta = \theta_A - \theta_I$, the S_{IA} segment can be expressed as:

$$S_{IA} = \frac{\Delta\theta - \sin\Delta\theta}{2} = \frac{(\Psi_{s,2} - \Psi_{s,1}) - \sin(\Psi_{s,2} - \Psi_{s,1})}{2} \quad \text{(A25)}$$

Substituting Eqs. (A21 and A25) into Eq. (A16), provides:

$$S_3 = S_{IAPB} + 2\, S_{IA} = \frac{n\,\sqrt{2}\,(m-a)}{2} + (\Psi_{s,2} - \Psi_{s,1}) - \sin(\Psi_{s,2} - \Psi_{s,1}) \quad \text{(A26)}$$

Once S_3 is known, substituting Eqs. (A13 and A26) into Eq. (A17) and using arctangent properties, after simple algebra, the area a_3 can be simplified, as well as the associated area A_3:

$$a_3 = \frac{1}{2}\left[\left(2\,(m-a) - \sqrt{2}\,n\right) a - \Psi_{S,1} + \Psi_{S,3}\right] \quad \text{(A27)}$$

$$A_3 = 8\,a_3 = 4\left[\left(2\,(m-a) - \sqrt{2}\,n\right) a - \Psi_{S,1} + \Psi_{S,3}\right] \quad \text{(A28)}$$

with m and n expressed by Eq. (9) and $\Psi_{S,3}$ equal to:

$$\Psi_{S,3} = arctan\frac{2\,a\,(a+m) - 1}{1 - 2\,a\,(a-m)} \quad \text{(A29)}$$

Area A2

The analytical solution of area a_2 can be derived by summing the area $S_{QIAA'}$ to the rectangle $S_{APP'A'} = a\,(x_P - x_Q)$ and subtracting the already calculated area S_3 (Eq. (A26)):

$$a_2 = S_{QIAA'} + a\,(x_P - x_Q) - S_3 \quad \text{(A30)}$$

To determine $S_{QIAA'}$, the coordinate of point Q (Fig. 1b) is needed (Eq. (21)), since $S_{QIAA'}$ can be expressed as:

$$S_{QIAA'} = \int_{x_Q}^{x_A} \sqrt{1 - (x - 2\,a)^2}\,dx = \left|\frac{1}{2}\left[(x - 2\,a)\,\sqrt{1 - (x - 2\,a)^2} - \operatorname{asin}(2\,a - x)\right]\right|_{x_Q}^{x_A} \quad \text{(A31)}$$

Solving Eq. (A31), which is a standard well-known integral, and rearranging, $S_{QIAA'}$ can be derived:

$$S_{QIAA'} = \frac{1}{2}\left(\operatorname{asin} a - a\,\sqrt{1 - a^2}\right) \quad \text{(A32)}$$

Knowledge of Eq. (A32), and considering the x_P and x_Q coordinates (Eq. (21)), Eq. (A30) can be rewritten:

$$a_2 = \frac{1}{2}\left(\operatorname{asin} a - a\,\sqrt{1 - a^2}\right) + a\,\sqrt{m} - a^2 - S_3 \quad \text{(A33)}$$

Substituting Eq. (A26) into Eq. (A33) and rearranging made it possible to derive the partial area a_2 and A_2 in a compacted form similar to A_1:

$$a_2 = \frac{1}{2}\left[\left(2\,\sqrt{2}\,n - m\right) a + 2\,\Psi_{S,1} - \Psi_{S,2}\right] \quad \text{(A34)}$$

$$A_2 = 8\,a_2 = 4\left[2\,\Psi_{S,1} - \left(m - 2\,\sqrt{2}\,n\right) a - \Psi_{S,2}\right] \quad \text{(A35)}$$

where m and n are expressed by Eq. (14) and $\Psi_{S,2}$ by Eq. (A24).

Appendix B

Area A1

As for the partial area a_1 of square spacing, the partial area a_1 of equilateral triangular layouts (Fig. 1b) can be determined by Eq. (A1), considering S_1 and $\Delta\theta_I$ associated with the coordinate of the point I (Eqs. (31) and (32)):

$$S_1 = \overline{II'}\cdot\overline{OI'} = \frac{1}{4}\left(\sqrt{3}\,a - m\right)\left(3\,a - \sqrt{3}\,m\right) \quad \text{(B1)}$$

$$\Delta\theta_I = 2\,arctan\left(\frac{x_I}{2\,a - x_I}\right) = 2\,\Psi_{H,1} \quad \text{(B2)}$$

where, considering x_I coordinate (Eq. (31)), $\Psi_{H,1}$ can be expressed as:

$$\Psi_{H,1} = arctan\frac{\sqrt{3}\,a - m}{\sqrt{3}\,m + a} \quad \text{(B3)}$$

Substituting Eq. (B1 and B2) into Eq. (A1), and rearranging the area a_1 and that associated with the reference area, A_1, can be obtained:

$$a_1 = \frac{1}{2}\left[\left(\sqrt{3}\ a - m\right)\ a - \Psi_{H,1}\right] \tag{B4}$$

$$A_1 = 12\ a_1 = 6\left[\left(\sqrt{3}\ a - m\right)\ a - \Psi_{H,1}\right] \tag{B5}$$

Area A3

The partial area a_3 can be determined by adding to the area of the triangle S_3 with base $\overline{IB}$ and height $\overline{BP}$, the halved circle segment, $S_{seg,3}$, denoted by the central angles towards the points I and B, $\theta_{I'}$ and $-\theta_{I'}$, with their difference, $\Delta\theta_{I'} = 2\ \theta_{I'}$:

$$a_3 = S_3 - S_{seg,3} = S_3 - \frac{1}{2}\,\frac{\Delta\theta_{I'} - sin\Delta\theta_{I'}}{2} \tag{B6}$$

with:

$$S_3 = \overline{IB}\cdot\ \overline{BP} = \frac{1}{2}(y_P - y_I)(x_P - x_I) = \frac{1}{24}\left(3\ \sqrt{3} - 2\ a\left(\sqrt{3}\ a + 3\ m\right)\right) \tag{B7}$$

$$\Delta\theta_{I'} = 2\ arctan\left(\frac{x_P - x_I}{y_{C2} - y_I}\right) = 2\ arctan\ \ \Psi_{H,3} \tag{B8}$$

where $\Psi_{H,3}$, considering the ordinate of the wetted circle centred in $C2$, y_{C2} (Fig. 6), and I and P coordinate (Eqs. (31) and (32)), can be expressed as:

$$\Psi_{H,3} = arctan\frac{\sqrt{3}\ m - a}{\sqrt{3}\ a + m} \tag{B9}$$

substituting Eq. (B7 and B8) into Eq. (B6) and rearranging, provides the partial area a_3 and the corresponding area, A_3:

$$a_3 = \frac{1}{2}\left[\left(\frac{a}{\sqrt{3}} - m\right)\ a + \Psi_{H,3}\right] \tag{B10}$$

$$A_3 = 12\ a_3 = 6\left[\Psi_{H,3} - \left(m - \frac{a}{\sqrt{3}}\right)\ a\right] \tag{B11}$$

Area A2

The partial area a_2 can be determined by subtracting the already calculated partial area a_3 to the trapezoid area $S_2(I'IPP')$ (Fig. 2b), and by adding the halved circle segment, $S_{seg,2}$, already considered in Eq. (B6):

$$a_2 = S_2 - a_3 + \frac{1}{2}\,\frac{\Delta\theta_{I'} - sin\Delta\theta_{I'}}{2} \tag{B12}$$

Considering the P and I coordinate (Eqs. (31) and (32)), the area S_2 can be written:

$$S_2 = \frac{(y_P - y_I)(x_P - x_I)}{2} = \frac{1}{24}\left(18\ a\ m - \sqrt{3}\left(3 + 2\ a^2\right)\right) \tag{B13}$$

Substituting Eq. (B8, B10, and B13) into Eq. (B12), and rearranging the partial area a_2 and the corresponding A_2, are derived:

$$a_2 = \frac{1}{2}\left[\left(2\ m - \sqrt{3}\ a\right)\ a + \Psi_{H,2}\right] \tag{B14}$$

$$A_2 = 12\ a_2 = 6\left[\Psi_{H,2} - \left(\sqrt{3}\ a - 2\ m\right)\ a\right] \tag{B15}$$

with $\Psi_{H,2}$ equal to:

$$\Psi_{H,2} = arctan\frac{2\ a^2 - 1}{2\ a\ m} \tag{B16}$$

References

Abd El-Wahed, M. H., Medici, M., & Lorenzini, G. (2016). Sprinkler irrigation uniformity: Impact on the crop yield and water use efficiency. *Journal of Engineering Thermophysics, 25*(1), 117–125. https://doi.org/10.1134/S1810232816010112

AL-Kayssi, A. W., & Mustafa, S. H. (2016). Modeling gypsifereous soil infiltration rate under different sprinkler application rates and successive irrigation events. *Agricultural Water Management, 163*, 66–74. https://doi.org/10.1016/j.agwat.2015.09.006

Amer, K. H. (2006). Water distribution uniformity as affected by sprinkler performance. *Misr J. Ag. Eng, 23*(1), 82–94.

Andrade, L. M., Pacheco, J. C. C., Costa, G. L. L., Alencar, C. A. B. D., & Cunha, F. F. D. (2022). Uniformity of water distribution by a sprinkler irrigation system on a soccer field. *Bioscience Journal, 38*, Article e38012. https://doi.org/10.14393/BJ-v38n0a2022-57028

Baiamonte, G., Vaccaro, G., & Palermo, S. (2024). Closed circuits of drip laterals versus open circuits: hydraulic performance and energy-saving potential. *Irrigation Science, 43*(6), 1255–1271. https://doi.org/10.1007/s00271-024-00981-z. . (Accessed 17 October 2024)

Baiamonte, G., & Vaccaro, G. (2026). Normalised numerical analysis of uniformity coefficients for a newly referenced sprinkler area under square and equilateral triangle spacing arrangements. *Biosystems Engineering.* , Article 104343. https://doi.org/10.1016/j.biosystemseng.2025.104343

Carriço, N., Felícissimo, D., Antunes, A., & Luz, P. B. D. (2025). Simulating water application efficiency in pressurized irrigation systems: A computational approach. *Water, 17*(8), 1217. https://doi.org/10.3390/w17081217

Chen, R., Li, H., Wang, J., Guo, X., & Xiang, Y. (2023). Evaluating soil water movement and soil water content uniformity under sprinkler irrigation with different soil texture and irrigation uniformity using numerical simulation. *Journal of Hydrology, 626*, Article 130356. https://doi.org/10.1016/j.jhydrol.2023.130356

Chen, R., Li, H., Wang, J., & Song, Z. (2023). Critical factors influencing soil runoff and erosion in sprinkler irrigation: Water application rate and droplet kinetic energy. *Agricultural Water Management, 283*, Article 108299. https://doi.org/10.1016/j.agwat.2023.108299

Christiansen, J. E. (1942). Irrigation by sprinkling. In *, Vol. 4. Agricultural experiment station Berkeley, CA, USA*.

Dechmi, F., Playán, E., Cavero, J., Faci, J. M., & Martínez-Cob, A. (2003). Wind effects on solid set sprinkler irrigation depth and yield of maize (Zea mays). *Irrigation Science, 22*(2), 67–77. https://doi.org/10.1007/s00271-003-0071-9

Fukui, Y., Nakanishi, K., & Okamura, S. (1980). Computer evaluation of sprinkler irrigation uniformity. *Irrigation Science, 2*(1), 23–32. https://doi.org/10.1007/BF00285427

García Bandala, M., Robles Rovelo, C. O., Bautista-Capetillo, C., González-Trinidad, J., Júnez-Ferreira, H. E., Servín Palestina, M., Pineda Martínez, H., Morales De Avila, H., & Rivas Recendez, M. I. (2022). Analysis of irrigation performance of a solid-set sprinkler irrigation system at different experimental conditions. *Water, 14*(17), 2641. https://doi.org/10.3390/w14172641

Hussain, Z., Liu, J., Chauhdary, J. N., & Zhao, Y. (2024). Evaluating the effect of operating pressure, nozzle size and mounting height on droplet characteristics of rotating spray plate sprinkler. *Irrigation Science*. https://doi.org/10.1007/s00271-024-00982-y

Keller, J., & Bliesner, R. D. (1990). *Sprinkle and trickle irrigation*. Springer US. https://doi.org/10.1007/978-1-4757-1425-8

Lehrsch, G. A., & Kincaid, D. C. (2010). Sprinkler irrigation effects on infiltration and near-surface unsaturated hydraulic conductivity. *Transactions of the ASABE, 53*(2), 397–404. https://doi.org/10.13031/2013.29579

Li, N., Liu, J., Zhou, N., Yang, Q., Liang, J., Li, J., Yu, L., Liu, X., & Zhang, W. (2022). Characteristics of rotary sprinkler water distribution under dynamic water pressure. *Horticulturae, 8*(9), 804. https://doi.org/10.3390/horticulturae8090804

Li, Y., Bai, G., & Yan, H. (2015). Development and validation of a modified model to simulate the sprinkler water distribution. *Computers and Electronics in Agriculture, 111*, 38–47. https://doi.org/10.1016/j.compag.2014.12.003

Li, J., & Kawano, H. (1996). Sprinkler rotation nonuniformity and water distribution. *Transactions of the ASAE, 39*(6), 2027–2031. https://doi.org/10.13031/2013.27705

Li, J., & Rao, M. (2003). Field evaluation of crop yield as affected by nonuniformity of sprinkler-applied water and fertilizers. *Agricultural Water Management, 59*(1), 1–13. https://doi.org/10.1016/S0378-3774(02)00123-3

Lu, Y., Liu, P., Montazar, A., Paw U, K.-T., & Hu, Y. (2019). Soil water infiltration model for sprinkler irrigation control strategy: A case for tea plantation in Yangtze River Region. *Agriculture, 9*(10), 206. https://doi.org/10.3390/agriculture9100206

Mantovani, E. C., Villalobos, F. J., Organ, F., & Fereres, E. (1995). Modelling the effects of sprinkler irrigation uniformity on crop yield. *Agricultural Water Management, 27*(3–4), 243–257. https://doi.org/10.1016/0378-3774(95)01159-G

Mateos, L., Mantovani, E. C., & Villalobos, F. J. (1997). Cotton response to non-uniformity of conventional sprinkler irrigation. *Irrigation Science, 17*(2), 47–52. https://doi.org/10.1007/s002710050021

Merriam, J. L., & Keller, J. (1978). *Farm irrigation system evaluation: A guide for management*.

Montazar, A., & Sadeghi, M. (2008). Effects of applied water and sprinkler irrigation uniformity on alfalfa growth and hay yield. *Agricultural Water Management, 95*(11), 1279–1287. https://doi.org/10.1016/j.agwat.2008.05.005

Nascimento, A. K., Schwartz, R. C., Lima, F. A., López-Mata, E., Domínguez, A., Izquiel, A., Tarjuelo, J. M., & Martínez-Romero, A. (2019). Effects of irrigation uniformity on yield response and production economics of maize in a semiarid zone. *Agricultural Water Management, 211*, 178–189. https://doi.org/10.1016/j.agwat.2018.09.051

Pan, X., Jiang, Y., Li, H., & Qin, L. (2023). Experimental research on the jet-breaking characteristics and hydraulic performance of a novel automatic rotating sprinkler. *Water Supply, 23*(5), 1935–1952. https://doi.org/10.2166/ws.2023.097

Pan, X., Jiang, Y., Li, H., & Zhou, X. (2024). Hydraulic performance of the rotational damping sprinkler: Analysis of the force acting on diffuser tooth I. *Irrigation and Drainage, 73*(1), 29–49. https://doi.org/10.1002/ird.2859

Playán, E., Zapata, N., Faci, J. M., Tolosa, D., Lacueva, J. L., Pelegrín, J., Salvador, R., Sánchez, I., & Lafita, A. (2006). Assessing sprinkler irrigation uniformity using a ballistic simulation model. *Agricultural Water Management, 84*(1–2), 89–100. https://doi.org/10.1016/j.agwat.2006.01.006

Playán, E., Zapata, N., Latorre, B., Cavero, J., Paniagua, P., Medina, E. T., Lorenzo, M. A., & Burguete, J. (2024). Ador-Solid-Set: A coupled simulation model for commercial solid-set irrigated fields. *Agricultural Water Management, 295*, Article 108740. https://doi.org/10.1016/j.agwat.2024.108740

Qureshi, W. A., Xiang, Q., Xu, Z., & Fan, Z. (2023). Study on the irrigation uniformity of impact sprinkler under low pressure with and without aeration. *Frontiers in Energy Research, 11*, Article 1135543. https://doi.org/10.3389/fenrg.2023.1135543

Rezayati, A. M., Liaghat, A., Sharifipour, M., & Ghameshlou, A. N. (2023). The importance of water depth distribution maps in the sprinkler irrigation system performance assessment. *Water Supply, 23*(11), 4425–4435. https://doi.org/10.2166/ws.2023.256

Robles, O., Latorre, B., Zapata, N., & Burguete, J. (2019). Self-calibrated ballistic model for sprinkler irrigation with a field experiments data base. *Agricultural Water Management, 223*, Article 105711. https://doi.org/10.1016/j.agwat.2019.105711

Salmerón, M., Urrego, Y. F., Isla, R., & Cavero, J. (2012). Effect of non-uniform sprinkler irrigation and plant density on simulated maize yield. *Agricultural Water Management, 113*, 1–9. https://doi.org/10.1016/j.agwat.2012.06.007

Santos, F. L., Reis, J. L., Martins, O. C., Castanheira, N. L., & Serralheiro, R. P. (2003). Comparative assessment of infiltration, runoff and erosion of Sprinkler irrigated soils. *Biosystems Engineering, 86*(3), 355–364. https://doi.org/10.1016/S1537-5110(03)00135-1

Seginer, I. (1987). Spatial water distribution in sprinkle irrigation. In *Advances in irrigation*. https://doi.org/10.1016/B978-0-12-024304-4.50006-7, 4, pp. 119–168). Elsevier.

Singh, V. P., & Su, Q. (2022). *Irrigation engineering: Principles, processes, procedures, design, and management*. Cambridge University Press.

Skhiri, A., Gabsi, K., Dewidar, A. Z., & Mattar, M. A. (2023). Artificial neural networks versus multiple Linear regressions to predict the Christiansen uniformity coefficient in sprinkler irrigation. *Agronomy, 13*(12), 2979. https://doi.org/10.3390/agronomy13122979

Stambouli, T., Zapata, N., & Faci, J. M. (2014). Performance of new agricultural impact sprinkler fitted with plastic nozzles. *Biosystems Engineering, 118*, 39–51. https://doi.org/10.1016/j.biosystemseng.2013.11.002

Tarjuelo, J. M., Montero, J., Carrion, P., Honrubia, F., & Calvo, M. (1999). Irrigation uniformity with medium size sprinklers part II: Influence of wind and other factors on water distribution. *Transactions of the ASAE, 42*(3), 677–690.

Tarjuelo, J. M., Montero, J., Honrubia, F. T., Ortiz, J. J., & Ortega, J. F. (1999). Analysis of uniformity of sprinkle irrigation in a semi-arid area. *Agricultural Water Management, 40*(2–3), 315–331. https://doi.org/10.1016/S0378-3774(99)00006-2

Tarjuelo, J. M., Montero, J., Valiente, M., Honrubia, F., & Ortiz, J. (1999). Irrigation uniformity with medium size sprinklers part I: Characterization of water distribution in no-wind conditions. *Transactions of the ASAE, 42*(3), 665–676.

Yang, F., Jiang, Y., Li, H., Hui, X., & Xing, S. (2024). Accurate model development for predicting sprinkler water distribution on undulating and mountainous terrain. *Computers and Electronics in Agriculture, 224*, Article 109196. https://doi.org/10.1016/j.compag.2024.109196

Zhang, L., Merkley, G. P., & Pinthong, K. (2013). Assessing whole-field sprinkler irrigation application uniformity. *Irrigation Science, 31*(2), 87–105. https://doi.org/10.1007/s00271-011-0294-0

Zhang, L., Merkley, G. P., Wu, P., & Zhu, D. (2018). Effect of Catch-Can spacing on calculation of sprinkler irrigation application uniformity. *CLEAN – Soil, Air, Water, 46*(7). https://doi.org/10.1002/clen.201800130

Zhu, X., Fordjour, A., Agyen Dwomoh, F., Kwame Lewballah, J., Anim Ofosu, S., Liu, J., Dai, X., & Oteng, J. (2024). Experimental study on the effects of pressure loss on uniformity, application rate and velocity on different working conditions using the dynamic fluidic sprinkler. *Heliyon, 10*(5), Article e27140. https://doi.org/10.1016/j.heliyon.2024.e27140